Simulation and Emulation of Water spray for Validation of Optical Sensors (SEVVOS)

Public report

Project within: FFI – Trafiksäkerhet och Automatiserade Fordon (TSAF)
Authors: Peter Eriksson (AZ), Erik Ronelöv (AZ), Mari Eriksson (AZ), Jan-Erik Källhammer (Magna), Paul Otxoterena (RISE), Valery Chernoray (Chalmers)

Date: 2025-01-24

Fordonsstrategisk Forskning och Innovation

1. Content

2. Summary

This research investigated visibility degradation caused by vehicle-generated water spray on wet surfaces, using experimental tests, simulations, and data analysis to examine spray dynamics and their effects on camera and sensor performance.

Dynamic tests faced challenges with automated contrast analysis due to insufficient resolution, lack of camera calibration, and poor lighting. Targets were too small in images, and low contrast, even without spray, prevented reliable detection. Similar issues affected static tests, although higher light levels enabled more consistent results. High-beam headlights worsened contrast degradation by illuminating spray particles. These findings emphasized the importance of proper calibration, resolution, and lighting for accurate data collection.

Outdoor tests on AstaZero test tracks showed that water depth and vehicle speed significantly influence spray and visibility. Deeper water (e.g., 9–10 mm) caused greater contrast degradation than shallower water (e.g., 4–5 mm), while higher speeds amplified spray effects, particularly in shallow water. Variations in light conditions affected the results, with clearer patterns emerging under stable lighting.

Tyre rig tests provided detailed measurements of aerosol and water spray properties, such as droplet size, density, and distribution. Smaller droplets (mode below 50 µm) formed near the tyre surface, while larger droplets developed downstream due to coalescence and aerodynamic forces. Higher tyre speeds and more water increased spray density and contrast degradation. In deeper water, contrast degradation was more uniform, with narrower ranges between maximum and minimum values.

Simulations revealed key mechanisms of spray generation and propagation. Water film depths as low as 100 µm produced spray through capillary adhesion, with droplets interacting with vehicle components and airflow. Larger droplets returned to the ground quickly, while smaller droplets remained suspended, affecting visibility. Data collected under naturalistic conditions validated these findings and provided insights into real-world visibility challenges.

This research highlights the critical role of water depth, vehicle speed, and spray dynamics in visibility degradation. It underscores the need for improved measuring methods, lighting, and testing protocols to enhance automated analysis and sensor performance, especially for autonomous vehicle systems in adverse weather conditions.

3. Sammanfattning på svenska

Detta projekt undersökte hur vattenspray från fordon på våta vägbanor påverkar siktförhållanden för fordonssensorer. Genom experimentella tester, simuleringar och dataanalys granskades sprayens dynamik och dess effekter på kameror och sensorer.
De dynamiska testerna stötte på problem med automatiserad kontrastanalys på grund av låg upplösning, avsaknad av kamerakalibrering och bristfälligt ljus. Kontrast-tavlorna var för små och kontrasten, även utan spray, var för låg för att möjliggöra pålitlig detektion. Statiska tester uppvisade liknande problem, även om bättre ljusförhållanden gav mer konsekventa resultat. Det visade sig att helljus förvärrade kontrastförlusten genom att lysa upp vattendropparna i sprayen. Dessa insikter betonade vikten av rätt mätmetoder, högre upplösning och bättre belysning för noggrann datainsamling.
Utomhustester på AstaZeros testbanor visade att vattendjup och fordonshastighet påverkar sprayen och sikten markant. Djupare vatten (9–10 mm) orsakade större kontrastförlust jämfört med grundare vatten (4–5 mm). Högre hastigheter förstärkte också sprayens effekter, särskilt vid grunt vatten. Variabla ljusförhållanden påverkade resultaten, men tydligare mönster framträdde under stabila ljusförhållanden.
Tester med en däckrigg gav detaljerade mätningar av vattensprayens egenskaper, såsom droppstorlek, densitet och fördelning. Mindre droppar (under 50 µm) bildades nära däckytan, medan större droppar utvecklades längre bort på grund av koalescens och aerodynamiska krafter. Högre däckhastigheter och större vattendjup ökade aerosolernas densitet och kontrastförlust. Vid djupare vatten blev kontrastförlusten mer jämn, med mindre skillnad mellan högsta och lägsta värden.
Simuleringar visade på viktiga mekanismer bakom sprayens bildande och spridning. En vattenfilm så tunn som 100 µm kunde skapa spray genom kapillär vidhäftning, där droppar interagerade med fordonets komponenter och luftflöden. Större droppar föll snabbt tillbaka till marken, medan mindre droppar förblev svävande och påverkade sikten. Data insamlade under naturliga förhållanden bekräftade dessa resultat och gav ytterligare insikter om verkliga utmaningar för sikten.
Forskningen belyser hur vattendjup, fordonshastighet och spraydynamik bidrar till försämrad sikt. Den understryker behovet av förbättrade mätmetoder, bra ljusförhållanden vid tester och optimerade testprotokoll för att förbättra automatiserade analyser av sensorers prestanda, särskilt för autonoma fordon i krävande väderförhållanden.

4. Background

This project was funded by FFI and conducted by AstaZero together with RISE, Magna and Chalmers. It is also affiliated to the AI-SEE project [1], co-labelled under the Penta Call 5/Euripides² Call 13, sharing knowledge and results with the European automotive industry as well.

Despite significant investments in automated vehicle technology, including spectacular demonstrations and widespread publicity, many challenges remain. Industry is still striving to achieve Automated Drive (AD) vehicles and Advanced Driver Assistance Systems (ADAS) that function reliably under all conditions. If the vehicles' Operational Design Domain (ODD) must be limited to driving only in daylight and favourable weather, much of the potential benefits of AD and ADAS will be lost. Systems that can safely handle autonomous driving in all conditions and on all roads are critical for a complete and successful market introduction.

Reproducing weather conditions reliably and repeatably poses a significant challenge for vehicle manufacturers, sensor developers, and testing environments. The project aimed to develop methods for virtually recreating water spray from surrounding vehicles, in sensors. Wet roads has been identified as a major issue for camera sensors, which are a crucial component of vehicles' perception systems [2]. By creating virtual water spray in camera sensors, already collected data can be used to improve sensor algorithms, ultimately enabling driving in adverse weather conditions. The challenge with creating virtual water spray for testing of camera-based perception systems lies in validating it against real water spray as experienced by sensors on actual roads.

Methods for recreating water spray are primarily found in enclosed, controlled environments such as wind tunnels or weather chambers, where parameters like light, wind, and water quantity can be kept consistent for each test. However, due to the advanced test setup, the cost of use is high, posing a limitation for vehicle and sensor developers. Another drawback is that the vehicle remains stationary throughout the test series. For most development testing, this type of validation becomes unsustainable, increasing the need for alternative testing methods.

The SEVVOS project aimed to develop new testing methods for realistically recreating water spray in semi-open environments, such as at the AstaZero test site. To achieve this, data collected by sensors mounted on vehicles will be used to recreate critical and severe situations through simulation, replayed as scenarios at AstaZeros test track and spray rig. A significant focus of the project was to create water spray that is realistic enough for vehicle-specific camera sensors. The project will address questions such as:

- What parameters must be considered when recreating a water spray scenario?
- How can a water spray rig be calibrated to produce realistic and repeatable water spray for camera sensors?

The project is parallel and connected to the AI-SEE project. Consequently, the results will contribute to enhancing research and innovation capacity, ensuring the competitiveness of the automotive industry and securing jobs in Sweden. Through the involvement in AI-SEE it also, mutually, presents and shares knowledge and results with the AI-SEE partners. By advancing expertise in weather generation, AstaZero will help develop internationally connected and competitive research and innovation environments in Sweden. Additionally, through the participation of Magna (former Veoneer), RISE, and Chalmers, the project fosters collaboration between industry, universities, and institutes.
This project contributes to the subprogram's roadmap as follows:

- **Program Area A – Analysis, Knowledge, and Enabling:** SEVVOS has developed knowledge in measuring and producing repeatable spray, analysing spray data in different situations to enable the development of perception systems in adverse weather.
- **Program Areas E and F – Intelligent and Collision-Avoidance Systems and Vehicles, and Automated Vehicles in the Transport System:** Development of methods and access to virtual and physical infrastructure to ensure the verification and validation of advanced driver assistance systems and autonomous vehicles under various weather conditions.

Previous feasibility studies and projects related to this subject have been conducted both at AstaZero, Magna (Veoneer), and RISE, as well as internationally. The Swedish projects funded by Vinnova, Spray1, Spray2, Weather Generation at AstaZero and SUS [2,4,5,6] have provided a better understanding of the challenges posed by spray from wet roads, highlighting that spray is more challenging than rain for vehicle-specific, primarily optical, sensors. Clear data on visibility degradation (contrast) has been obtained from both real and artificial spray, created using a dedicated spray rig.
Although these projects clarified the issues surrounding water spray and its impact on sensors, they did not propose many solutions. This project aims to assist sensor manufacturers in developing their sensors by creating repeatable and controlled spray that is carefully characterized as realistic enough for the sensors.
Internationally, partners in the AI-SEE project have undertaken initiatives such as Adose, PReVENT, HAVEit, MiniFaros, Artrac, AdaptIVe, RobustSENSE, and DENSE [8,9,**Error! Reference source not found.**,10,11,12,13,14] to improve sensor performance in adverse weather or visibility conditions. While these projects have succeeded in enhancing vehicle visibility in fog, detecting snowbanks, and improving visibility depth and pedestrian detection in fog, they fall short of supporting SAE Level 3 driving. Therefore, more work is required in sensor development and data fusion validation.
Globally, some research has been conducted on sensor performance under poor weather conditions and how it might be improved. Additionally, studies on airflow dynamics and water droplet behaviour behind vehicles on wet roads—particularly how a vehicle's own spray affects it, such as contamination—have been undertaken. To validate the proposed test method, further research is needed on the characteristics of droplets in spray, including their size, quantity, and distribution, which are not yet extensively documented.

In the earlier mentioned FFI projects at AstaZero, measurements have primarily been performed using various contrast panels and cameras, with contrast as a metric representing the difference in light intensity between black and white squares. This has provided a solid understanding of how much camera data is degraded by water spray and suggests that the equipment used to create artificial spray could be refined to produce even more realistic but primarily repeatable water spray for sensor testing.

The FFI project SUS focused on developing the spray rig to facilitate further research into the effects of water spray. It emphasized the rig's development and understanding contrast measurements and contrast degradation caused by spray produced by the rig compared to real vehicles.

A previous project, *"Physical characteristics of spray clouds produced by heavy vehicles (trucks and lorries) driven on wet asphalt,"* [15] was conducted by RISE and AstaZero in 2020. The results give a good insight into the droplet characteristics in real-world spray and the report is publicly available online. This study utilized various optical measurement techniques such as shadowgraphy and light extinction measurements to characterize water spray created by a truck with and without a trailer traveling at a constant speed on wet asphalt.

5. Purpose, research questions and method

This project continues where the rig's development ended in SUS, focusing on creating concrete measurement methods and calibrating the rig. Together with industry, institutes, and universities, we aim to achieve tangible results to assist the industry (including Magna) in further developing better optical sensors for autonomous driving and ADAS. Using the equipment and methods developed in the project, along with RISE's extensive expertise in the field, we aimed to refine and improve the methodology to better define the spray generated by the rig.

The project tried to answer key questions, such as:

- What parameters must be considered when recreating a water spray scenario?
- How can a water spray rig be calibrated to produce realistic and repeatable water spray for automotive sensors?

The project partners further developed the methodology and approach for creating artificial water spray to simulate real road conditions when driving on wet roads. A large amount of field data was collected by Magna using a vehicle equipped with six different types of cameras. This vehicle was also used to validate the methods at AstaZero.

The spray rig, developed under the SUS project, was further refined and calibrated to replicate real-world water spray conditions in a repeatable and controlled way. Validation was conducted by comparing artificial spray with real-world data using metrics such as contrast degradation.

Still, the simulations and measurements support the assumption that the spray created sufficiently replicates real-world conditions.

6. Objective

Through this project, the partners aimed to strengthen collaboration with the Technical University of Ingolstadt's Center of Automotive Research on Integrated Safety Systems and Measurement Area (CARISSMA), which participated in AI-SEE, to further enhance Sweden's expertise in this research field. The SEVVOS project aimed to strengthen the spray rig and testing methods developed by AstaZero and Magna, particularly among major European vehicle manufacturers such as Mercedes. By participating in AI-SEE, the Swedish partners could influence the development of simulations and the artificial creation of adverse visibility conditions. This collaboration was crucial for establishing a more uniform testing methodology across participating countries and partners.

Participation in AI-SEE allowed the Swedish partners to help shape the direction of development in the simulation and artificial creation of adverse visibility conditions.

The completed spray rig developed in the SUS project served as a demonstrator, and a demonstration of the complete equipment at AstaZero was performed as part of AI-SEE toward the end of the project. Publications from Chalmers on simulations and AstaZero on the testing method were performed.

Building on insights from previous European projects like DENSE, the partners within AI-SEE anticipated that the outcomes of AI-SEE and this project would enable the generation of training data for AI under poor weather and visibility conditions. This was to be achieved by utilizing both existing and newly collected data from adverse weather and visibility conditions. These methods for simulated spray were intended to be verified and further developed with physical spray artificially produced by the rig. This provided significant opportunities to explore machine learning and neural networks as tools for safer traffic, both nationally and internationally.

This approach could help eliminate the need for extensive data collection in specific weather conditions across different locations worldwide. Consequently, lead time, costs, and environmental impact can be significantly reduced.

In collaboration with AI-SEE and drawing from lessons learned in previous European projects, which included major international stakeholders in the field, the solutions developed here have the potential for a significant market impact.

7. Results and deliverables

Within the project there has been several test campaigns on the AstaZero test site and at RISE in Borås, but also data collection campaigns by Magna and computer simulations at Chalmers. All these are summarized with one chapter each in chronologic order.

7.1. Proof of Concept with 3M-tape

Date: 2022 June 20-22nd ***Place***: AstaZero Garage Area
Attendees: Peter Eriksson (AZ), Erik Ronelöv (AZ), Oscar Tullberg (AZ), Valery Chernoray (CTH), Antoine Carreau (CTH), Antoine Jallon (CTH), Ruslan Moldagazyyev (CTH), Jan-Erik Källhammer (Veoneer/Magna)
Test Vehicle: Lync & Co 01

Background

To collect data on real spray from vehicles driving on a wet surface repeatably there needs to be a measurable and controllable water depth on the road surface in the tests. Many different methods have been discussed on this subject and at this event, we tested some of them.
The overall idea is to have a small barrier surrounding the test area that keeps the water in so that only a small amount of water must be re-applied after each test. The materials used cannot leave any marks on the surface after the tests that could ruin testing for other customers. This has proven to be more challenging than anticipated, as the asphalt is far from smooth, and the barrier must withstand being driven over multiple times. On top of that, the barriers must be safe for the driver if the car would skid on the road during tests from hydroplaning for example. All requirements were summed up in a list as follows:

- Overridable, especially the short edges (even at high speeds)
- No residue or other damage on the test surface
- Watertight seal to the surface
- Minimum leakage
- Not oppose any danger to the driver in the event of hydroplaning
- Not too complicated or expensive due to the large amounts needed
- Short setup time
- Max height needed, 20 mm
- Nice to have - applicable even on wet surface

Different solutions

Absorbing materials: Rope, textile or sandbags can be portable and easy to apply and are overridable if kept within reasonable size/height. But it is unlikely that they will contain the water, and it will be a lot of work to take care of all the wet products after the tests.
Delimiting solutions: Some sort of weight like a plank or similar with a foam or rubber material underneath could contain the water. However, driving over planks or similar at high speed could not be considered safe and the ability to contain water is questionable.
Enveloping solutions: By placing some sort of roofing felt, floor mat or similar on the ground with something underneath along the edges a sort of pool can be created. This might be easy to make watertight but unclear if it will hold up when worn by the car tyres. This would also need a lot of materials, and it is not a real road surface to drive on so it could be considered unsafe.

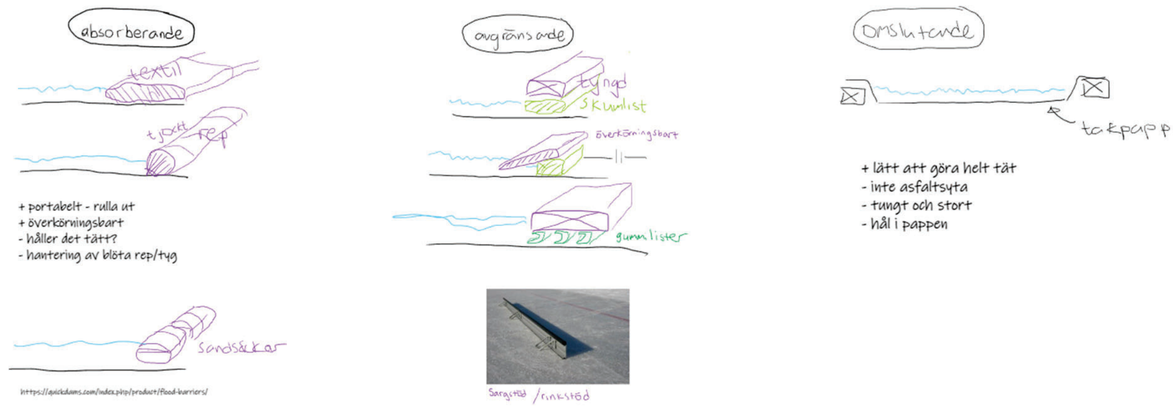

Figure 1 - Sketches of different solutions for water barriers

Figure 2 - Functional tests of different materials

Test setup

Different combinations of tapes and barriers were taped on dry asphalt and then water was applied to determine how well they could contain the water.
The best solution proved to be a delimiting solution using heavy duty tape from 3M that was taped on the asphalt to create a watertight bond and then a regular LAN cable was taped on top of it with a double-sided tape to act as a barrier. This solution was then used to create a 5x20 meter square.
Due to the slope of the surface (approximately 1%) it was impossible to fill the whole square with water with a barrier of only 8 mm. The water gathered in a long puddle along the side of the square that was lowest.
Some passes were made with the car, but the speed allowed on the used test area is only 30 kph so very little spray was created.


Figure 4 - Partially filled 5x20m square barrier


Figure 3 - Little spray generated in 30 km/h

Conclusions

Because of the slope of the surface, it is better to create one water pool for each wheel track and the pool can be made deeper and wider by using a thicker barrier.
A long spirit level or similar can be used to find the best spot on a test area to conduct the tests. The barriers should be placed so that the surface slopes to one side.
At the speed these few tests were performed, most of the water was displaced by the front wheels when they entered the puddles. Not much spray was created behind the vehicle. This was expected but spray generation was not the main purpose of this campaign.

7.2. Tape tests on Multilane Road

Date: 2022 August 29-30th ***Place***: AstaZero Multilane Road
Attendees: Peter Eriksson (AZ), Erik Ronelöv (AZ), Paul Otxoterena (RISE)
Test Vehicle: Lync & Co 01

Background

Conclusions from the tests performed in June 2022 along with literature studies and other conceptual tests performed in the daily work were used to decide on the layout for this test campaign.
We knew that we needed higher speeds, higher barriers and a relatively long wet area. The tape barriers should be placed in relation to the slope of the test surface and create one long puddle for each wheel track.

Test setup

Two U-shaped "pools" are created on the Multilane Road (MLR) track using the special tape from 3M with a rope underneath to form a barrier approximately 10-12 mm high to hold water. Water is continuously added from the left side, and because the track slopes from left to right relative to the driving direction, the water remains in the "puddles". The puddles are approximately 20 meters long, with a water depth of about 8-10 mm at the wheels. In the final third of these pools, two contrast targets are positioned on the western side, one facing south and the other east. Detectors for laser extinction measurements are also set up in the same area. In the south end of the pools another contrast target is placed facing north.
Just before the pools, a Lumix camera is placed, directed northward toward the contrast target facing south. This camera captures the degradation in contrast on the left side of the Vehicle Under Test (VUT) as it moves. A mirrored setup uses a Nikon camera placed after the pools directed towards the south contrast target.
On the eastern side of the lane, a GoPro camera is positioned to perform similar contrast measurements against the panel facing east. This setup provides a time-resolved, perpendicular cross-section of the spray generated by the VUT as it passes. In the same location, lasers for extinction measurements are also set up, complemented by a strong halogen spotlight aimed at the panel. The plan includes adding a high-speed camera to capture the shape and spread of the "spray plume" created by the VUT during its passage.

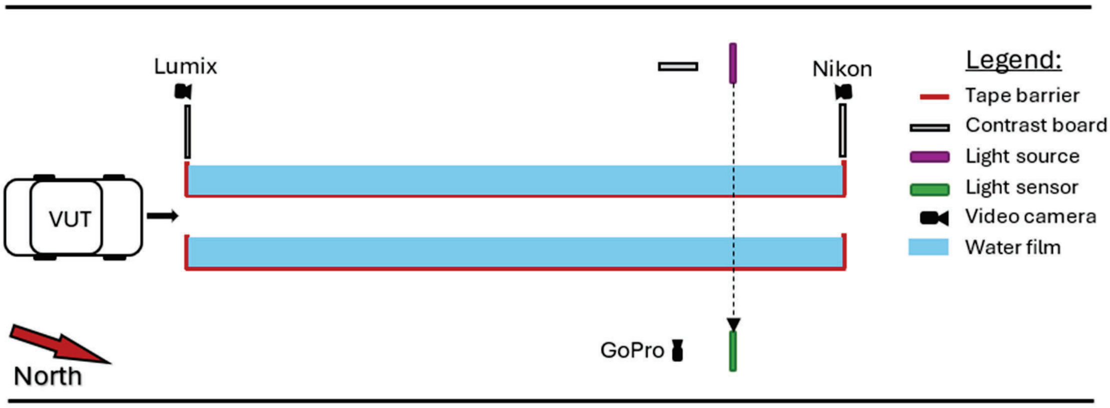

Figure 5 - Test setup for MLR

The speed of the VUT is set between 70 and 100 kph and the water depth is noted before passage for every test. The contrast measured is meant to be focused on the contrast degradation and not the actual contrast for every test, meaning the difference between contrast without spray before passage is compared with the contrast with spray during the passage.

Results

In total, 32 passes were made, 16 in each direction. The water was refilled occasionally so that multiple water depths were represented. The amount of water was documented on camera and then divided into 5 levels, 1-5 with 5 being the highest.
The collected data that was usable is summarized in the tables below.

Rows for different speeds and columns for different amounts of water with the contrast degradation from baseline in % shown in each cell in the left tables and number of video samples in the right tables.

Cm_Att - Lumix

	H20 = 1	H20 = 2	H20 = 3	H20 = 4	H20 = 5	AVG
70		1	17	3	65	21
80			38		72	55
90	6	4	24	29	50	23
100	3	15	7	6		8
AVG	4	7	21	13	62	

Number of runs

	H20 = 1	H20 = 2	H20 = 3	H20 = 4	H20 = 5	Tot
70	0	2	2	3	3	10
80	0	0	1	0	2	3
90	1	3	3	1	2	10
100	1	3	2	2	0	8
Tot	2	8	8	6	7	

Cm_Att - Nikon

	H20 = 1	H20 = 2	H20 = 3	H20 = 4	H20 = 5	AVG
70		11	25	16	46	24
80		13	47		76	46
90	54	27	33	33	40	37
100	10	28	16	30		21
AVG	32	19	30	26	54	

Number of runs

	H20 = 1	H20 = 2	H20 = 3	H20 = 4	H20 = 5	Tot
70	0	2	2	3	2	9
80	0	1	1	0	2	4
90	1	3	3	1	2	10
100	1	3	2	2	0	8
Tot	2	9	8	6	6	

Contrast degradation in relation to speed

- Few data points in 80 kph
- Largest contrast degradation in 80 kph
- Smallest contrast degradation in 100 kph for both cameras
- Large difference between cameras in 100 kph

	Lumix		Nikon	
kph	**Samples**	**Average (%)**	**Samples**	**Average (%)**
70	10	21	9	24
80	3	55	4	46
90	10	23	10	37
100	8	8	8	21

Contrast degradation in relation to water depth

- Largest contrast degradation with the most water (5)
- Few samples with the lowest amount of water (1)
- Large difference between cameras at lower water levels

	Lumix		Nikon	
Water level	**Samples**	**Average (%)**	**Samples**	**Average (%)**
1	2	4	2	32
2	8	7	9	19
3	8	21	8	30
4	6	13	6	26
5	7	62	6	54

Conclusions

As usual in these kinds of campaigns, not all test runs generated useable data but in total 31 video files from each camera could be used for analysis. The occasional water refill, camera issues and other smaller issues lead to different numbers of log files for each speed and water depth. Overall, we realized that too few data points were created to make any real statistically valid conclusions.

7.3.FFI Demo

Date: 2023 July 7th ***Place***: AstaZero FLX Zone
AstaZero conducted a demo for FFI and some other attendees at FLX Zone at the AstaZero test site. The current Spray Rig and software was presented for an interested audience.

Conclusion

When describing the random nature of the phenomena, the large impact of external influences and lack of substantial data sets with real-world data, it was clear that the complexity of this topic was unknown for several attendants.
Potential future costumers showed high interest in the topic and the ability to create sensor disturbances in a repeatable way. They also asked for future capabilities with contaminants, like salt or dirt, in the spray.

7.4.Tape tests on High Speed Area

Date: 2023 August 14-17th ***Place***: AstaZero, High Speed Area
Attendees: Peter Eriksson (AZ), Erik Ronelöv (AZ), Alfred Aronsson (AZ), Paul Otxoterena (RISE)
Test Vehicle: VW Caddy

Background

From the tests performed on the Multilane Road in August 2022 we knew that the water filled area needed to be longer and we needed to collect more samples to increase the credibility of the analysis. It was also clear that a more sophisticated method to determine the water depth was needed and that the number of different speeds should be kept to a minimum.
A long thorough discussion regarding what parameters were of importance lead to the setup used for the tests. Pros and cons for all selections were listed and investigated as much as possible to get the best possible results from the test.

Test setup

The parameter preparations lead to the following:

Vehicle
Even if no other vehicles are involved in the test, it is important to decide on a standard car that can be used again in future tests. The project settled for a VW Caddy.

Tyres
Due to the time frame the tyres used for the test will be the ones that are already on the car. It turned out to be fresh summer tyres on the car.

Speed
70 and 90 kph are selected because they were already used in a previous project done by RISE that produced good data [15]. Lower than that we suspected it would not produce enough spray, instead we added 120 kph to see if that is possible to drive in a safe way.

Direction
Driving in both directions would give possibilities to compare the two camera feeds in relation to incoming light but would also complicate the analysis with one more parameter. It was decided to only drive south to north.

Water
From the same project [15] we aim to reproduce water depths of 4, 7 and 9 mm with a lower priority on the highest number because it might produce too much splash.
The max depth is decided by the thickness of the barrier used including the 3M special tape. A 10 mm in diameter rope is used with the tape over it as shown in the figure below.

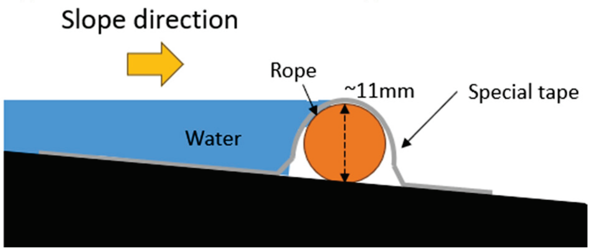

Figure 6 - Schematic of the slope angle and water depth

Taped pools
The width of the pools could be calculated with a 11 mm depth and a surface with 1% slope to be around 110 cm.
The length of the pools is settled to 50 m, one of for each tyre track placed with the same track width as the car.

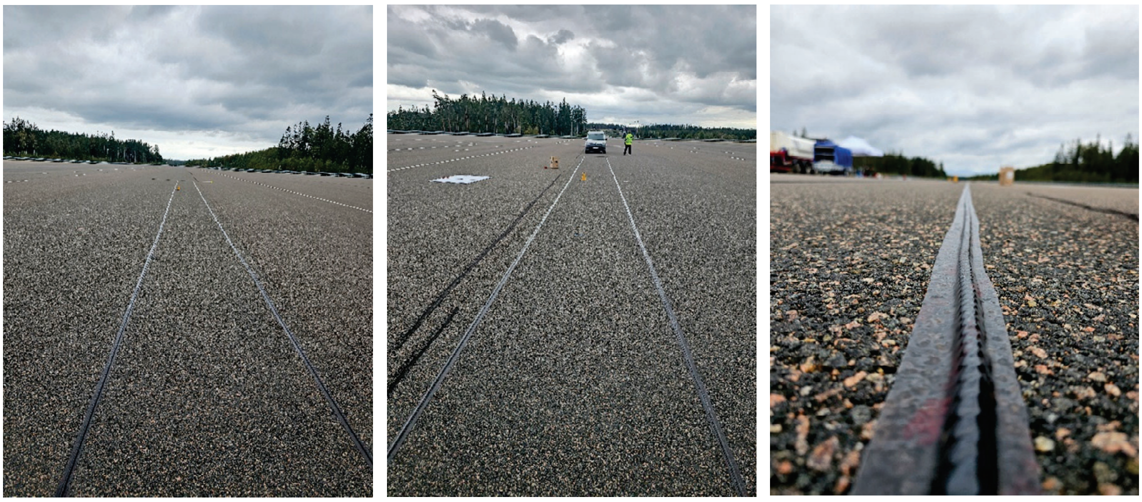

Figure 7 - The taped barriers on High Speed Area (HSA)

Target size

The checkerboard targets for the cameras in parallel to the test area (1 and 2) are 160x120 cm (WxH) and the target for the perpendicular camera (3) is 258x120 cm.

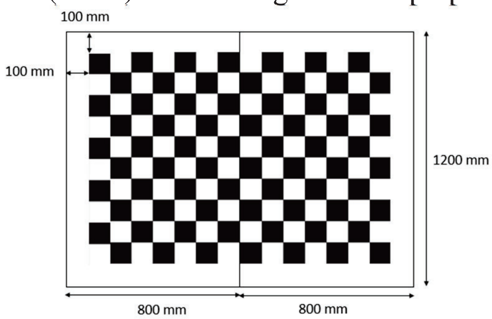

Figure 8 - Target 1 and 2

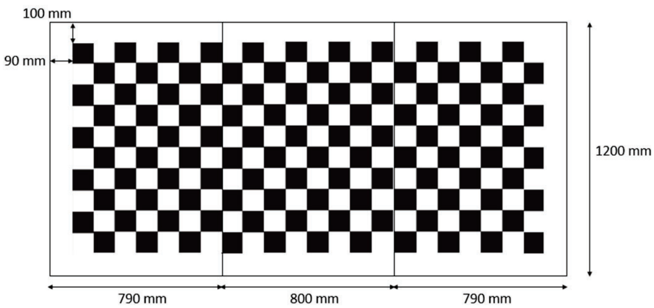

Figure 9 - Target 3

Target surface

The white areas of the targets are white forex board itself, and the black squares are from glossy vinyl. This is the same material used for all our contrast boards used in earlier projects as well.

Depth measurements
To get a fast measurement method for the water depth, long laminated paper rulers with coloured 10 cm areas are used. These targets are then filmed with regular GoPro cameras so that in the analysis it can be noted how far from the barrier the car was in every test sample. The slope of the surface dictates that the water depth decreases with 1 mm every 10 cm away from the barrier.


Figure 10 - Coloured ruler and passing car

Camera calibration
Using our calibration software, the Lumix cameras are regularly set to a decided contrast value without spray by tuning camera exposure settings.

Number of cameras
Two identical cameras are used to film its opposing checkerboard target through a hole in the middle of one of the middle black squares in the targets. This way we obtain data from both directions of the same spray event to see the impact of incoming light conditions. Zoom objectives are used so that the target fills as much as possible of the camera view.
One Sony camera with higher fps is placed in the middle of the test setup to film the larger checkerboard. This will give data on how long the spray plume is and some basic idea of how it looks.
As mentioned before, one GoPro camera is used to film each coloured ruler for depth estimation. So, three in total.

Camera placement
The Lumix cameras are placed 40 m apart so that there is 5 m of water film before the car enters the filmed area.
The cameras and targets are placed as close as possible to where the leftmost part of the water pool ends, without being in danger of getting hit by the car during tests, ~40 cm.

Surface
The wetted surface is high grade asphalt with smaller ballast than public roads (11 mm vs 16 mm) and a higher (dry) friction of 0,9-0,95 compared to 0,7-0,8 for regular roads. This made it easier to get the tape watertight on the surface.

Spectrometer
In the middle of the test area a strong light source with all wavelengths is placed perpendicular to the driving direction. On opposing sides of the wet area two spectrometers are placed, facing the light source.
Using an oscilloscope this can determine the droplet size distribution for the water spray.

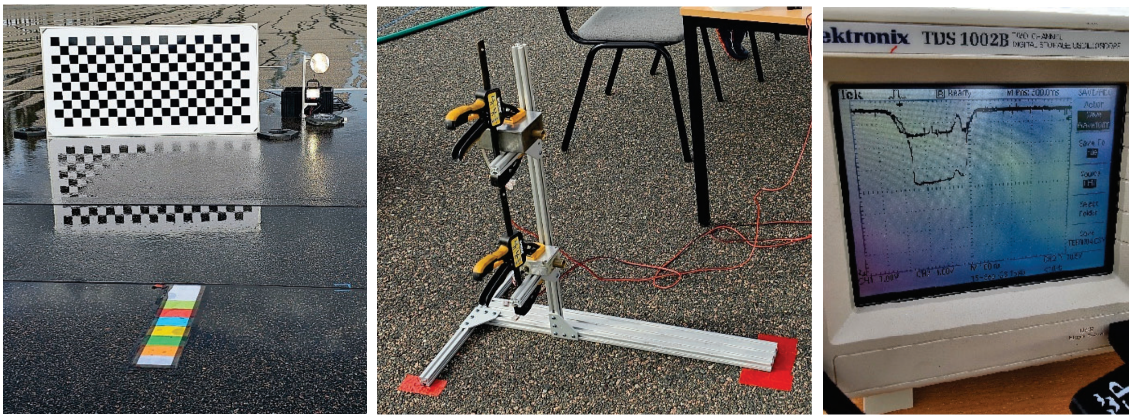

Figure 11 - Spectrometer setup with light source, sensors and oscilloscope

Incoming light
Some parameters can't be controlled. Incoming light is one of them and for that reason, lux measurements will be done continuously during the tests.

Wind
Another parameter that can't be controlled is the wind. In this case we must gamble and hope for as little wind as possible and especially not sideways due to the great effect it would have on the spray movement.

Rain
Just as for the wind, we must take a gamble here and hope for no precipitation. In case of rain, we will adapt the analysis in some way to take the rain into account.

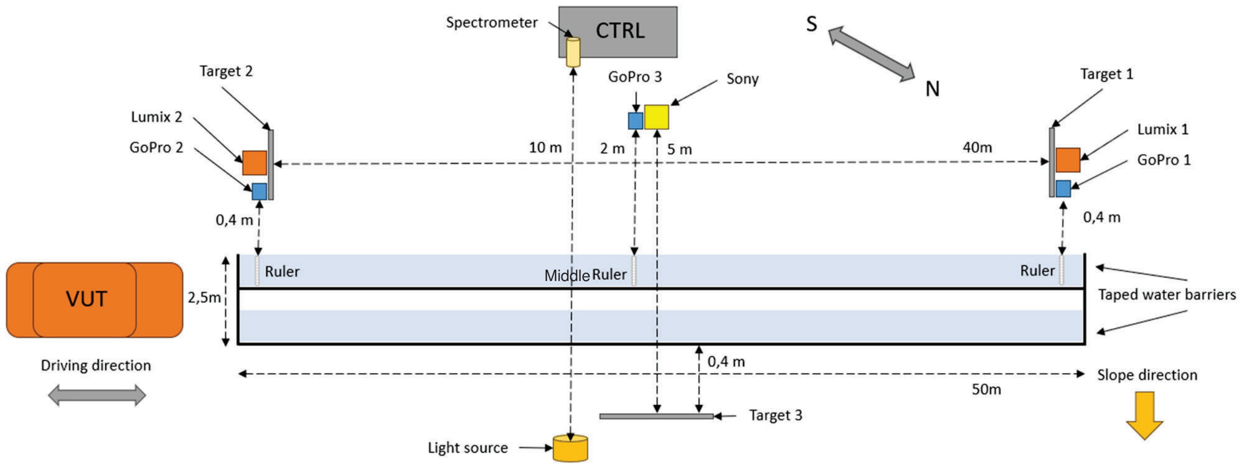

Figure 12 - Schematic of the whole setup for the tests on High Speed Area

Results

During the 15th all preparation work was done with taping the lines and putting up all targets and a tent with all computers and controls to monitor the tests.
All three days offered zero precipitation and a reasonably even overcast creating stable light conditions, even the wind was minimal. The line taping went faster than expected and looked promising.
To supply the test surface with water both a 1 m³ IBC tank and a 2 m³ metal tank with pumps and hoses were used. The main amount of water however was distributed with a water tank truck with a 16 m³ capacity and water sprinklers in the back. Every time the truck passed to fill up the water it was noted in the test log.
In total, 104 passes were made with the car. As in all testing, some of the data was not usable due to different reasons such as wind gusts, loose/shaking cameras, un-synced equipment and broken barriers. All 104 log files were still analysed. The analysis included running all video files from both Lumix cameras through our contrast analysis tool and determining the water depth by looking at all GoPro videos and note what colour the tyre passed through. After this is done all data from Lumix 2 could be plotted like below.

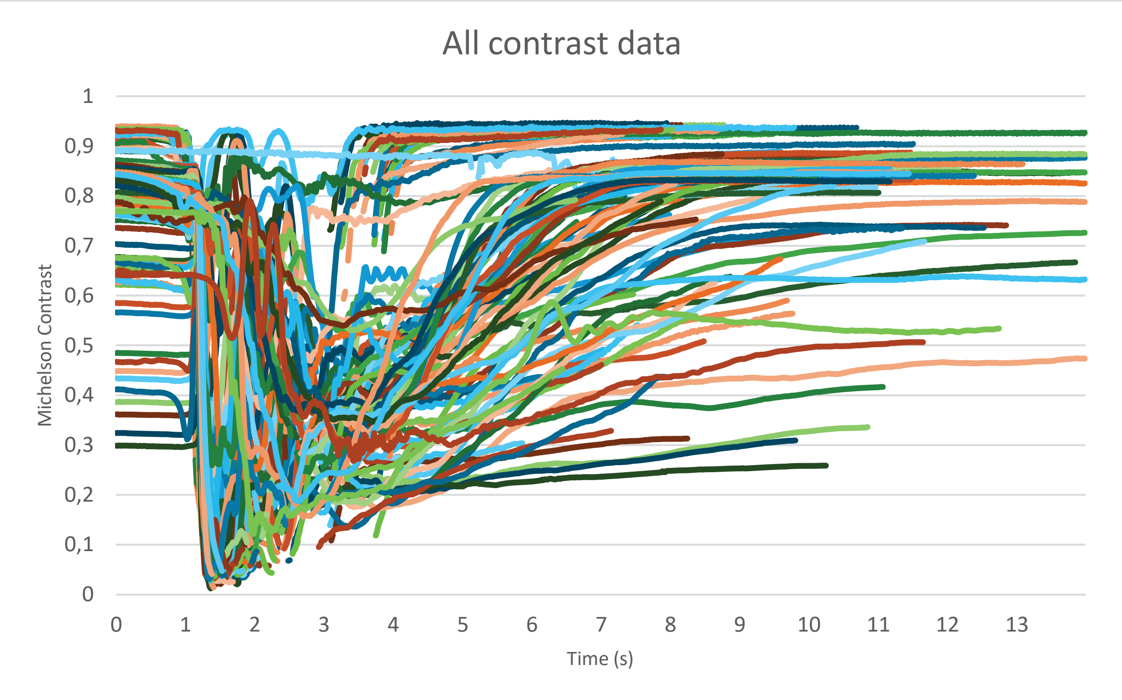

Figure 13 - Data for all test runs plotted together

All the unusable data was then removed, and the rest could be grouped in different ways to see how the contrast is affected by the spray generated by the car depending on speed and water depth.

Even though there are uncontrollable variables as light conditions and wind and the method for water depth measurements has some flaws, some patterns can be seen when comparing data. First, we compare data from the 16th (purple) with data from the 17th (green), all with 66-69 kph speed and 6-7 mm water depth. The difference in light conditions seems to be the main reason for the differences in data from the two test days since no other major changes were made.

The wave pattern that can be seen in much of the data is, from what we can see in the analysis, created by the heavy splash right next to or in front of the front wheel. In Figure 14 the first dip in contrast (1) is when the car enters the water, the second one (2) is the extra water gathered at the ruler in the middle of the water segments (as seen in Figure 12) and the third one (3) when the car passes the north checkerboard.

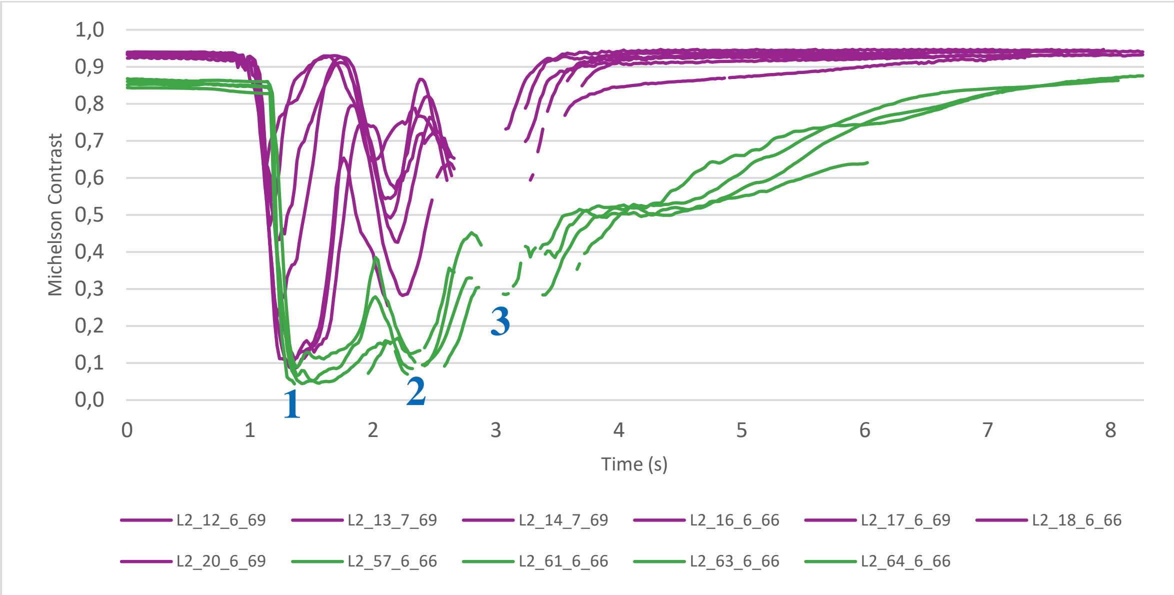

Figure 14 – Purple data is from the 16th and green from the 17th. Three clear "waves" can be seen

In the following comparisons the contrast data from 16/9 is grouped in 9-10 mm (red) and 6-7 mm (green) water depth, all in 66-69 kph speed. And then the same for data from 17/9 with 66 kph, 8 mm (red) and 4-5 mm (green) water depth.

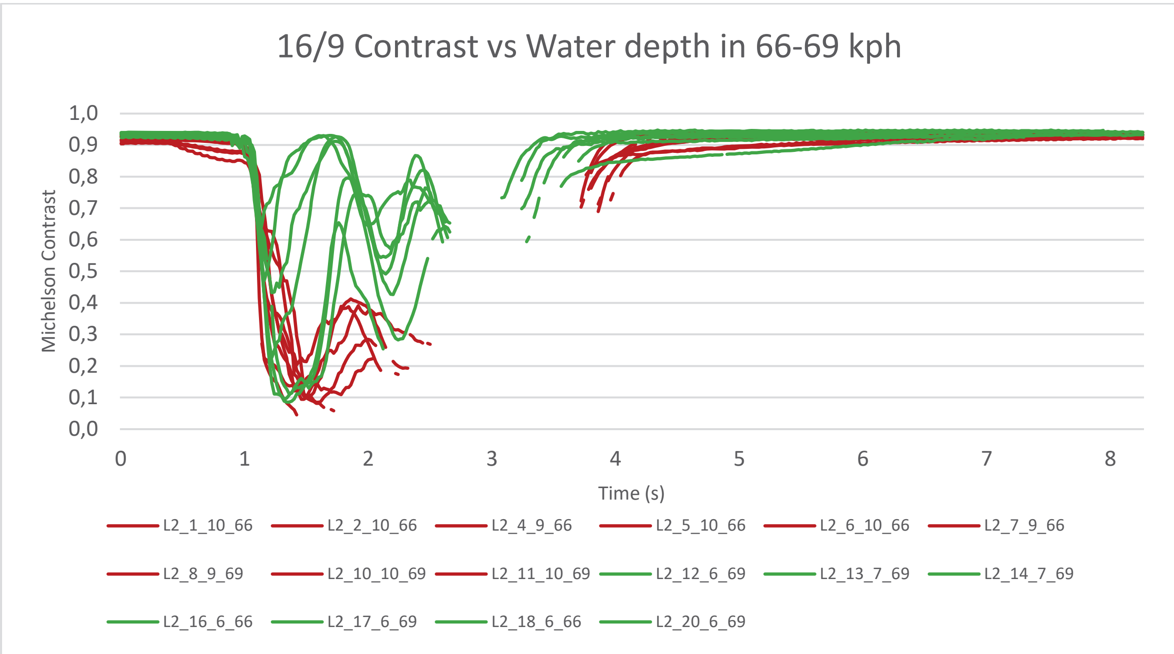

Figure 15 - Data series naming [Camera_Sample#_WaterDepth(mm)_Speed(kph)].

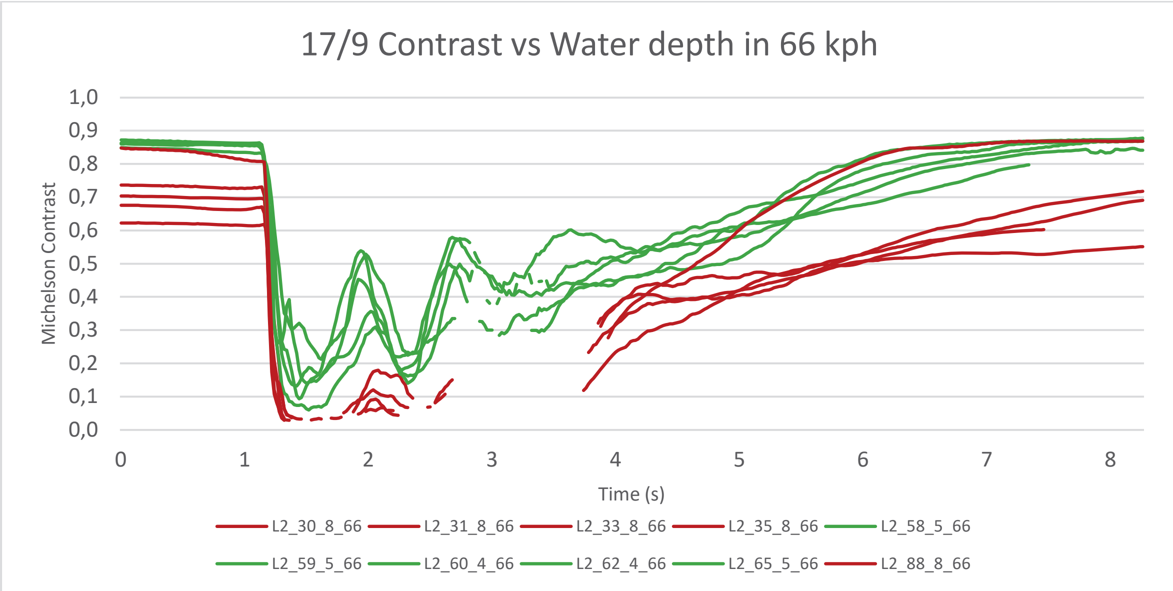

Figure 16 - Data series naming [Camera_Sample#_WaterDepth(mm)_Speed(kph)].

Judging by the plots we get a decent repeatability with the same parameters (speed and depth) with deeper water leading to a larger contrast degradation.
Below is contrast data from 17/9, first grouped in 66-69 kph (green) and 80-84 kph (red) speed, all in 4-6 mm water depth. And then the same day but grouped with 66 kph (green) and 84-116 kph (red) speed, all with 8 mm water depth.

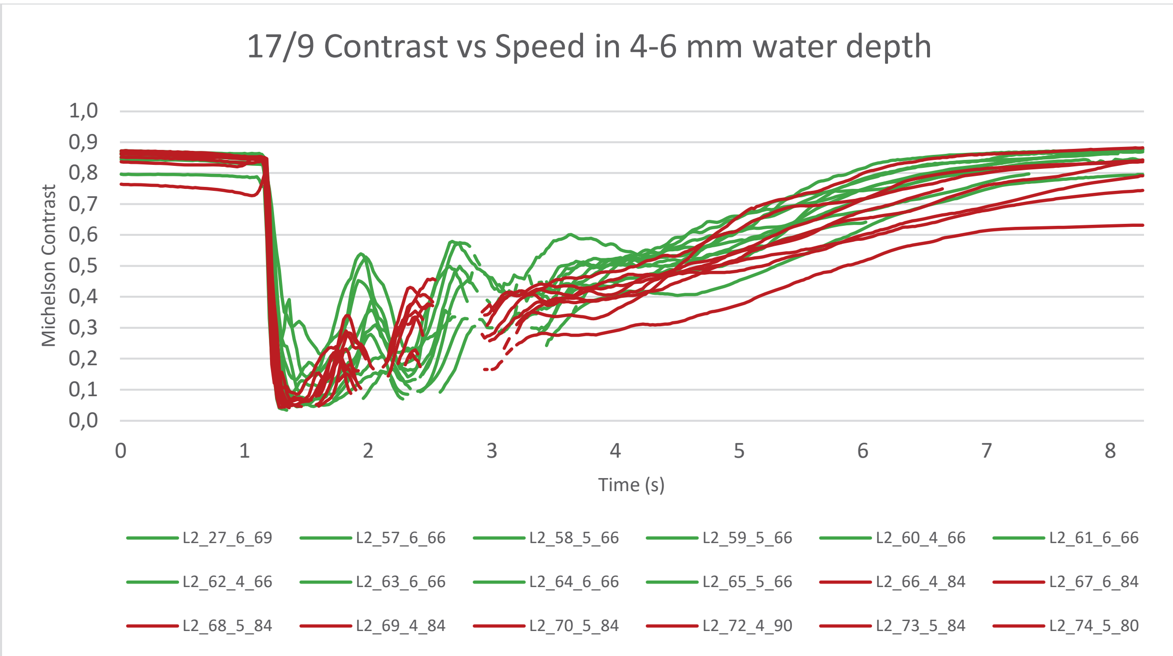

Figure 17 - Data series naming [Camera_Sample#_WaterDepth(mm)_Speed(kph)].

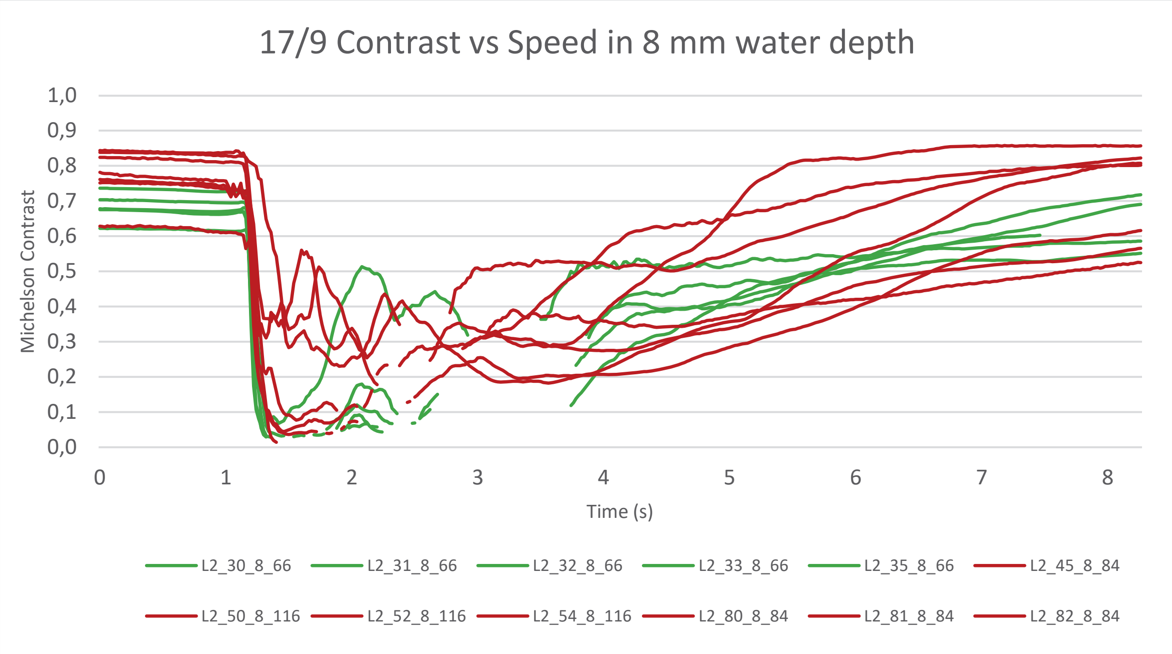

Figure 18 - Data series naming [Camera_Sample#_WaterDepth(mm)_Speed(kph)].

For 4-6 mm water the wave form is more eminent and the average contrast during spray is higher. For more water (8 mm) the differences are not that clear, at least not for the 12 samples collected here.

Conclusions

The study involved three days of testing under stable weather conditions, with no precipitation, minimal wind, and consistent overcast lighting. A water tank truck, supplemented by additional tanks and pumps, supplied the test surface with water. A total of 104 vehicle passes were conducted, with video and contrast data analysed from Lumix cameras and GoPro footage to assess water depth and spray effects.

Despite uncontrollable variables such as slight differences in light conditions and some limitations in the water depth measurement method, key patterns emerged. Data comparison between September 16th and 17th—focused on consistent speeds (66-69 kph) and water depths (6-7 mm)—revealed that light condition differences were the primary cause of variations. A distinct wave pattern in contrast data was linked to water splash dynamics, specifically at entry points, the midpoint ruler, and near the checkerboard.

Grouping data by water depth showed that deeper water (e.g., 9-10 mm) consistently resulted in greater contrast degradation compared to shallower depths (4-5 mm). Furthermore, increased vehicle speed amplified the spray effects, though the difference in contrast degradation between different speeds were clearer in shallower water (4-6 mm) than in deeper conditions (8 mm).

In conclusion, the results demonstrated a reasonable level of repeatability under consistent conditions, with clear correlations between water depth, vehicle speed, and contrast degradation. These findings provide a solid foundation for further studies on visibility impacts in wet road conditions.

7.5.Tyre rig tests

Date: 2023 December 11-15th ***Place***: RISE
Attendees: Peter Eriksson (AZ), Erik Ronelöv (AZ), Paul Otxoterena (RISE), Jan-Erik Källhammer (Magna)

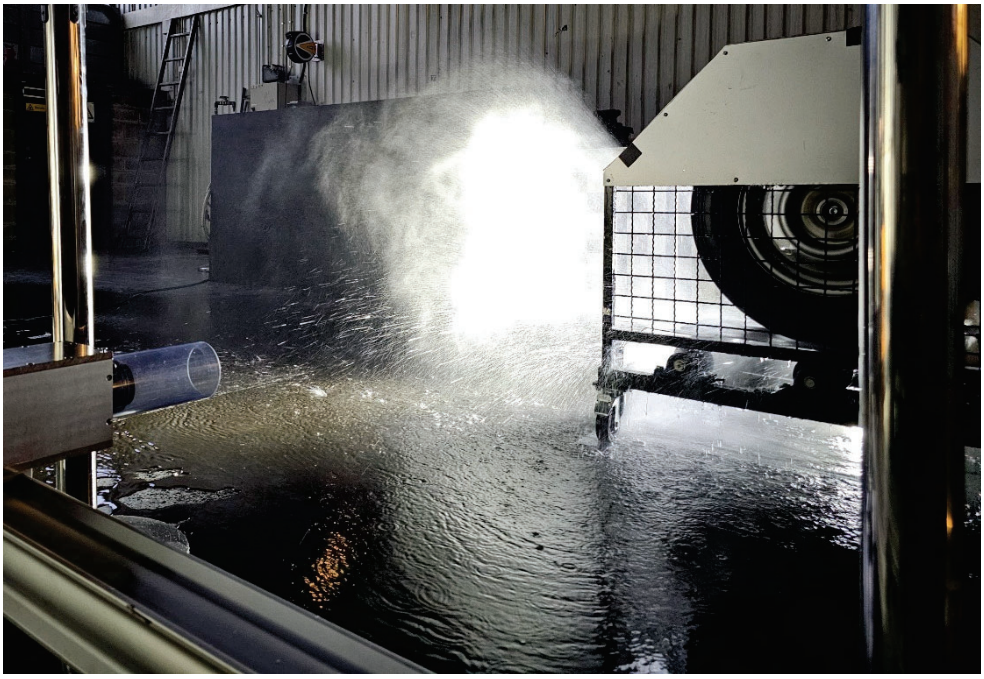

Figure 19 – Test setup for tyre rig spray test

The conclusions from the test campaign can found below and the full report "Characterisation and variabilities of sprays produced by tyres rotating on wet surfaces" can be found here [16].

Conclusions

Quantitative data of the physical characteristics of the aerosols produced by commercial tyres rotating on wet surfaces were measured by optical methods. Measurements of droplet size distribution, number density, and contrast degradation were conducted under controlled conditions in a test rig where water depth, rotational velocity, and tyre tread pattern were varied. Assessments were taken at various distances from the contact zone between the tyre surface and the tensioned belt.

Results pertaining 500 mm from the contact zone, show that in general the distributions are log-normal, with mode values below 50 µm, and that there are virtually no droplets exceeding 500 µm. Further, the cumulative distribution functions indicate that the droplet size at the 50th percentile (Dp 50 %) is approximately 100 µm, while the droplet size at the 90th percentile (Dp 90 %) is approximately 250 µm across all tested conditions.
Measurements taken 1000 mm downstream from the contact zone, generally reveal broader distributions with larger droplet sizes compared to those measured closer to the tyre surface. The droplet size at the 50th percentile (Dp 50 %) ranges between 150 and 200 µm, while the droplet size at the 90th percentile (Dp 90 %) ranges between 300 and 350 µm across all tested conditions. The largest droplets are nearly 600 µm, which is approximately 100 µm larger than those measured closer to the tyre surface. Results indicate that coalescence, as well as inertial and aerodynamic forces, play a significant role in the evolution of these aerosols.
Increasing the rotational velocity of the tyres, while maintaining the water depth, led to seven-to-eight-fold increase in the number density (Nd) and volume fraction (*fv*) of the aerosols from the summer tyres. An increase in aerosol number density and volume fraction was also observed when the rotational velocity of the tyres was increased from 70 to 110 km/h and the water depth was reduced from 0.75 to 0.5 mm. Near the tyre, the number density (Nd) and volume fraction (*fv*) had values ranging between 1 and 10 mm-3 and 5x10-3 and 30x10-3, respectively while far downstream the tyre, the number density (Nd) and volume fraction (*fv*) had values ranging between 0.2 and 2 mm-3 and 2 x10-3 and 15 x10-3, respectively.
Increasing the tyre's rotational speed while decreasing the water depth results in a reduction in the average contrast. Additionally, the range between the maximum and minimum contrast values becomes narrower under these conditions. When the water depth is increased while maintaining the rotational speed, the average contrast reaches its lowest values, and the interval between the maximum and minimum contrast values is at its smallest.

7.6.Spray tests with AstaZero Spray Rig V2

Date: 2024 June 14th ***Place***: AstaZero, DryZone
Attendees: Peter Eriksson (AZ), Erik Ronelöv (AZ), Mari Eriksson (AZ), Jan-Erik Källhammer (Magna)
Test vehicle: Magna multiple sensor carrier, Mercedes S-class.

Dynamic test setup

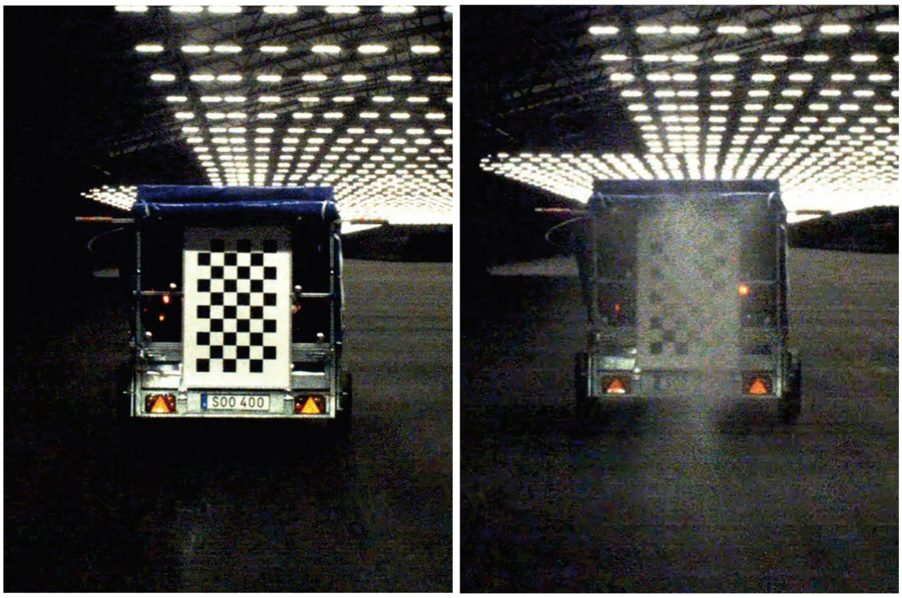

Figure 20 – Contrast target occluded by spray generated by the spray rig while driving in DryZone

Tests were done in DryZone at AstaZero with the Magna test vehicle and the dynamic spray rig in June 2024. The vehicle is equipped with a multitude of sensors for vehicle perception, such as polarized cameras, gated camera and IR camera.
A 60 by 120 cm checkerboard target was mounted on the back of the AstaZero Spray Rig V2, and the rig was set to produce spray with 2, 4 or 6 CAY spray nozzles*. The spray rig was then towed behind a car and the Magna test car followed on a distance were minimal spray landed on the sensor surfaces. Several runs were done with different spray amounts and all data from the sensor cluster was recorded to the onboard data storage. The idea was that all data (at least from regular camera and maybe gated camera) could be analysed with the dedicated contrast analysis tool developed by AstaZero. This would give a proof of concept for the dynamic spray rig in a very controlled environment inside the DryZone test area.

**CAY is a nozzle comprising of a cluster of 7 nozzles (CA) and it sprays in a wide angle (Y)*

Dynamic results

From AstaZeros point of view the tests were not very successful because the data could not be analysed in an automated manner. The automated tool needs to find the target to calculate contrast data and due to the lack of camera calibration the contrast, even without spray, was too low for the tool to find the target. Another reason that the target could not be automatically detected is that the target was too small in the picture leading to a low resolution on the actual target squares.

Results from the tests from Magna's point of view can be found in their report attached in Appendix A – Magna Report.

Static test setup

The same spray rig and test car were used for two static tests, also inside DryZone on the same day. The first one with the test car standing straight behind the spray rig, just like when driving behind, using the same spray settings as in the dynamic tests. In the second setup a larger checkerboard target was used, and the test vehicle was placed perpendicular to the spray rig with the checkerboard on the opposite side of the spray.

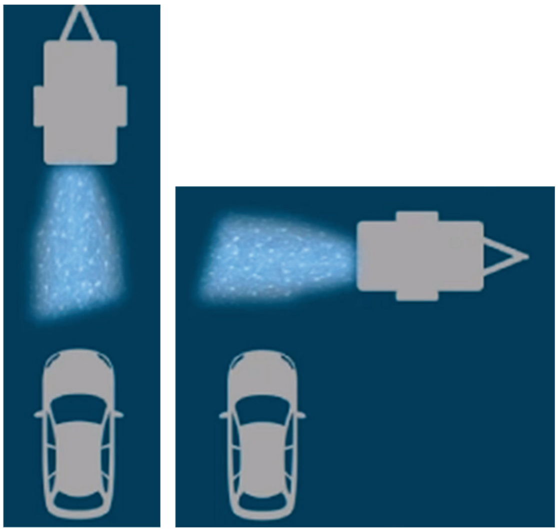

Figure 21 Insert caption here

Static results

When analysing the data it was clear that the tests from the first setup (straight behind) had the same issue as the dynamic tests. Too dark and too low resolution meant difficulties in automated analysis.

For the second setup, data was collected from two different places in DryZone. This led to some of the data being too dark and some having enough light. Five samples with the same water amount and nozzle setup are plotted below. At first investigation the input data seems identical but when plotting there are clear differences between them.

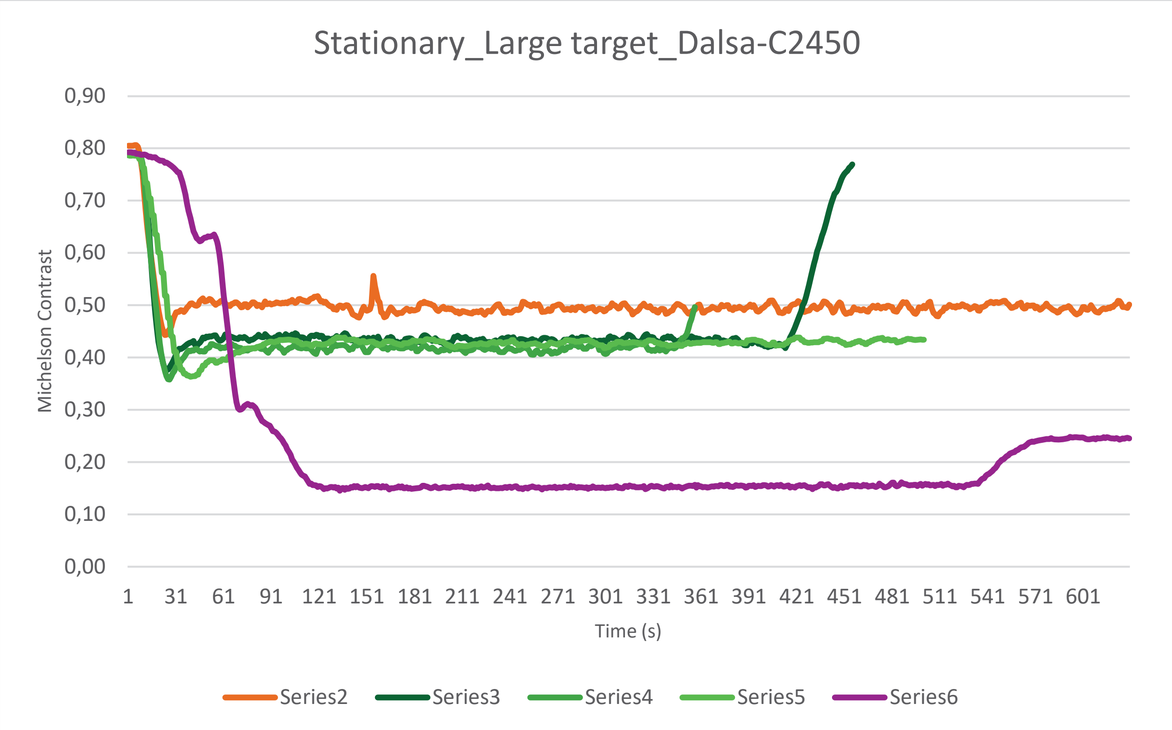

Figure 22 – Contrast data from the Magna test vehicle in static tests

The first sample (orange) has lower light conditions due to the placement in DryZone and that causes slightly less contrast degradation when spray is applied.

Three samples (green) are created at higher light conditions, and they show a repeatable contrast degradation when spray is applied.

In the fifth sample (purple) the headlights of the car are on high beam. This illuminates the spray particles, causing a higher contrast degradation than without the head lights.

Conclusions

The tests highlighted significant challenges with automated contrast analysis due to low camera resolution, lack of calibration, and insufficient lighting. In the dynamic tests, the automated tool failed to detect the target consistently, as the contrast without spray was too low, and the target's size in the images resulted in low resolution. Similarly, the first static test setup (straight behind) suffered from the same issues, making automated analysis difficult.
For both static and dynamic tests there are important differences that need to be considered for future tests. The measurement method used by AstaZero is not suitable for analysing video from the Magna cameras. The AstaZero method needs higher resolution and is more sensitive to the amount of lighting available. However, the AstaZero method is optimized for automation to extract contrast data from video from both moving and stationary video.
The second static setup provided more varied results. Data collected from two locations in DryZone showed differences in light conditions affecting contrast degradation. Lower light levels led to slightly less contrast degradation, while higher light levels allowed repeatable contrast degradation patterns when spray was applied. Additionally, high beam headlights illuminated spray particles, increasing contrast degradation compared to conditions without headlights.
These findings underscore the importance of proper lighting, resolution, and calibration for automated analysis of visibility degradation in spray conditions. While the results demonstrate repeatable patterns under specific conditions, improvements to the experimental setup and analysis tools are needed for more consistent and automated data processing.

7.7. Data Collection Events

The Data Collection set up is described in detail in Appendix A – Magna Report. There have been four main data collection events.

1. Winter tests, Muonio, Finland, 14-17 Feb 2023 213 GB
2. Spray on wet road, Vårgårda 8 Aug 2023 24 GB
3. Off-road, Padasjoki, Finland, 29-30 Aug 2023 82 GB
4. Artificial spray, AstaZero DryZone 17 June 2024 22 GB

Conclusions

A selection of adverse weather conditions under naturalistic conditions have been collected at a spectrum of conditions that may be encountered by a vehicle. It has generated an understanding of how obscurants in the atmosphere affect the captured image quality of on-board cameras and other sensors.

It has generated a database of image sequences that are available to all project partners.

7.8. Spray simulations

The Spray simulations is described in detail in Appendix B – Chalmers Report. Four different simulations are performed.

1. Spray Propagation Behind Vehicles
   - DES (Detached Eddy Simulation) captured realistic spray dispersion, while RANS (Reynolds-Averaged Navier-Stokes) failed to model unsteady flow effects.
   - Side wind deflected smaller droplets more than larger ones, affecting visibility and sensor performance.
2. Single Wheel Spray Simulations
   - 200 µm droplets matched previous CFD results, while 500 µm droplets aligned with experimental data.
   - Larger droplets settled quickly, whereas smaller droplets remained airborne, influencing spray cloud formation.
3. Truck Spray Simulations
   - Spray dispersed widely behind the truck, with larger droplets settling faster and smaller ones staying suspended.
   - DES provided better accuracy than RANS, showing realistic wake turbulence effects on spray movement.
4. Spray Visibility Modelling
   - Bulk light scattering models provided a practical approach to simulate spray impact on visibility.
   - Combined spray and rainfall significantly reduced visibility, affecting safe driving speeds and sensor performance.

Conclusions

These results enhance understanding of spray behaviour, sensor limitations, and road safety in wet conditions.

8. Evolution of the AstaZero Spray Rig

8.1.2021 - Spray rig from Magna (former Veoneer)

As described thoroughly in the final report for SUS [6]. Two sets of Kärscher M3 pressure washers in combination with spray nozzles from UltraFog and a large fan producing winds upwards of 65-70 kph. Water is provided via regular Gardena hose from the tap, maximum 15-16 lpm.
This rig was created by Veoneer in a previous project of theirs and loaned to AstaZero for the project SUS. It produces high pressure but a low volume of water. The addition of a large fan lets it mimic driving in water spray conditions while standing still.

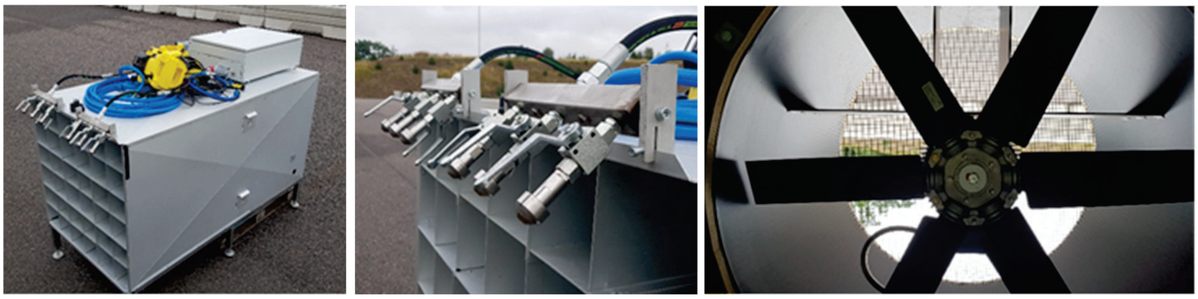

Figure 23 - Veoneer spray rig

8.2.2022 – AstaZero Spray Rig V1

The first own version of the AstaZero spray rig was created within the SUS project and described in detail in the final report for SUS [6].
This version of the rig consists of a standard trailer with a steel frame covered with a thick tarpaulin. Building on a trailer increases the mobility of the equipment significantly and enables dynamic testing with the trailer towed by a car in front of the test object.
The water system has a 250-litre water tank that is connected to a 200 Bar industrial pressure washer from Alcon with an integrated pump. The water outlet from the pump is divided into several quick release connections via dedicated ball valves to maximize flexibility and setup time. One of the outlets is connected to a precision adjustment valve with a manometer that is used to dump water back to the water tank and in that way adjust the flow going out of the other outputs.
Using the quick connections from the outlet different nozzles can be connected, both the UltraFog nozzles and other models from PNR Nordic were used.
After using this rig for a large part of the SUS project it was concluded that water volume

Figure 25 - AstaZero spray rig v1

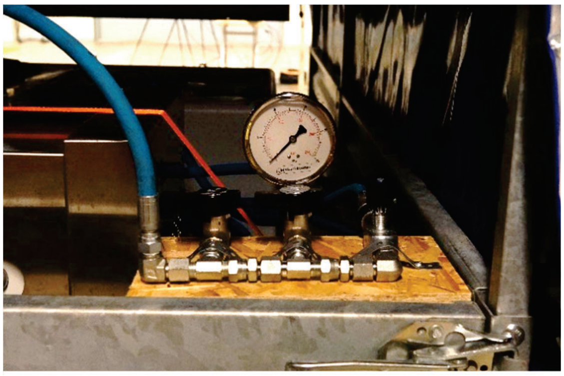

Figure 24 - Control panel for AstaZero spray rig v1

was more important than pressure to supply enough spray to do dynamic tests and spread the spray over a large enough volume using a larger number of nozzles at the same time.

8.3.2024 – AstaZero Spray Rig V2 (present)

The present version of the spray rig is mounted on the same trailer that was used in the previous version. This means that the old version does no longer exist.
It comprises of a centrifugal pump with a 230 l/m and 10 bar capacity connected to the same 250 l tank as before but now with 40 mm piping to facilitate higher flow rates.
The complete system comprises of multiple ball valves, manometers and adjustment nobs. In principle it has four "output channels", a main dump valve, one external refill connection and three adjustment points with manometers for pressure readings.
In standby mode the water is circulated from the tank, through the main dump valve and back into the tank via the return pipe.
In refill mode the pump will suck water from the external refill pipe via the main dump valve and into the onboard tank.
By opening any number of the four output channels and closing the main dump valve, different amounts of spray can be produced with attached nozzles (presently models DA, RX and CAY from PNR Nordic [16]). In the present setup there are two large CAY nozzles connected to each of the three tuneable channels and six different smaller nozzles connected to the fourth channel.

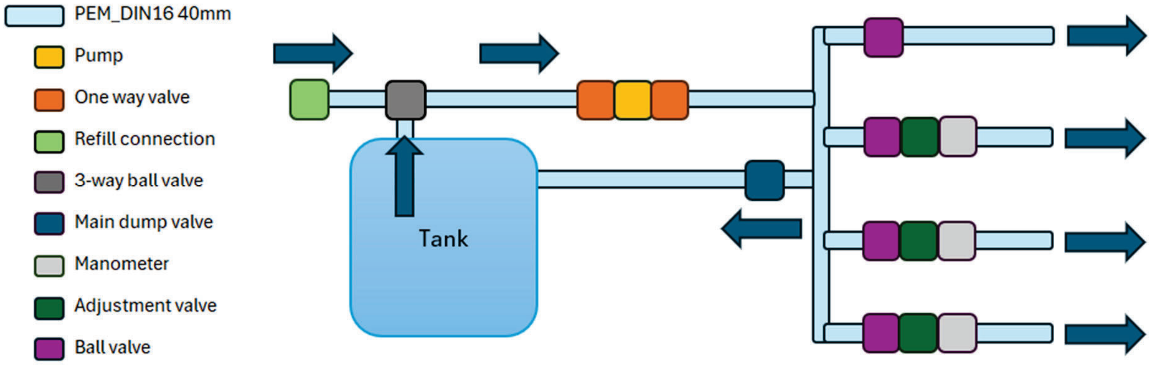

Figure 26 - Concept diagram of the AstaZero Spray Rig V2

A petrol generator is mounted in the trailer to supply power to the system during dynamic spray testing. In the present setup with all nozzles open full throttle the rig will consume upwards of 100 litres per minute, meaning just over 2 minutes of constant spray. However, the tank can be refilled with the onboard pump at a rate of over 200 litres per minute so by connecting to an external buffer tank the rig can be refilled in just a couple of minutes.

The following images show the spray rig without the tarpaulin cover before the petrol generator was mounted. A more user-friendly and reliable electrical setup is planned to be done in the near future.

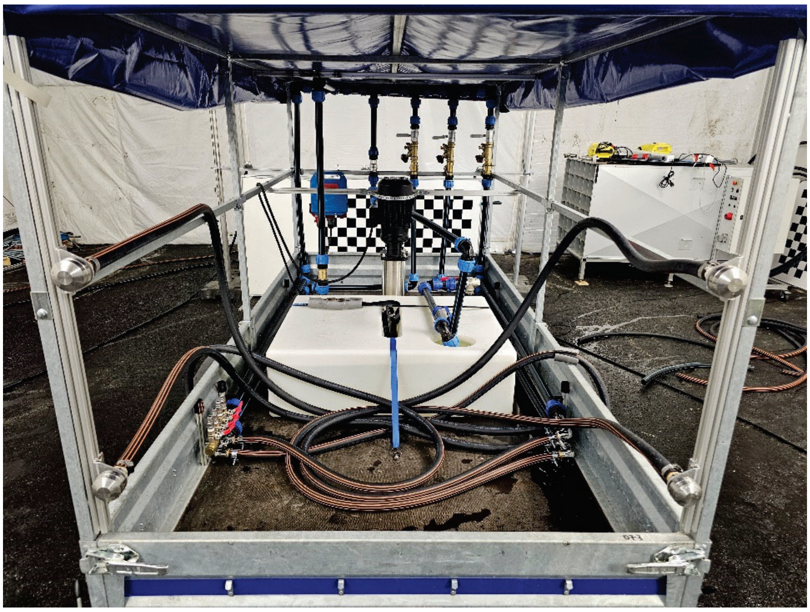

Figure 27 - Spray rig V2 without cover. Back view.

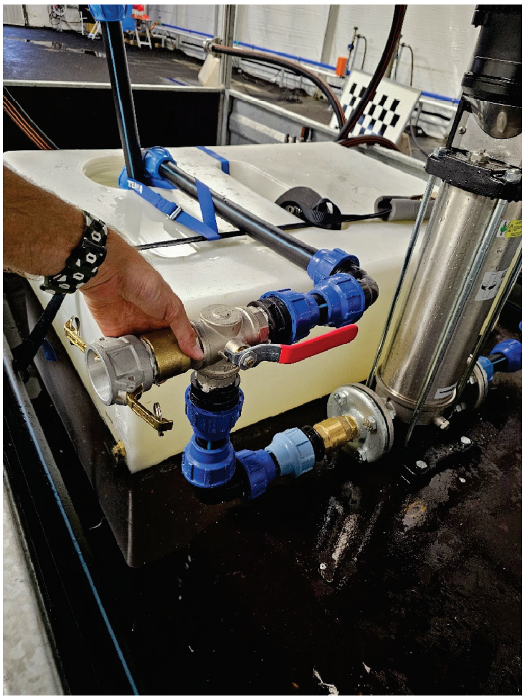

Figure 28 - Quick connection for external refill with 3-way ball valve.

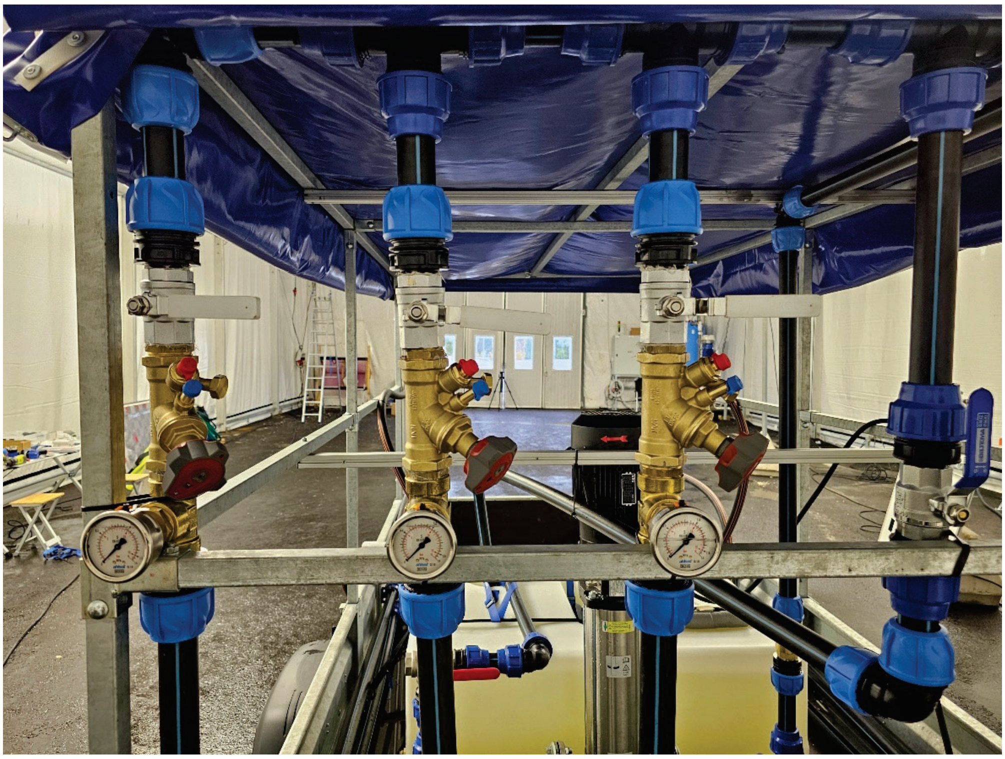

Figure 29 - Ball valves, adjustment valves and manometers for 3 channels and main dump valve (right).

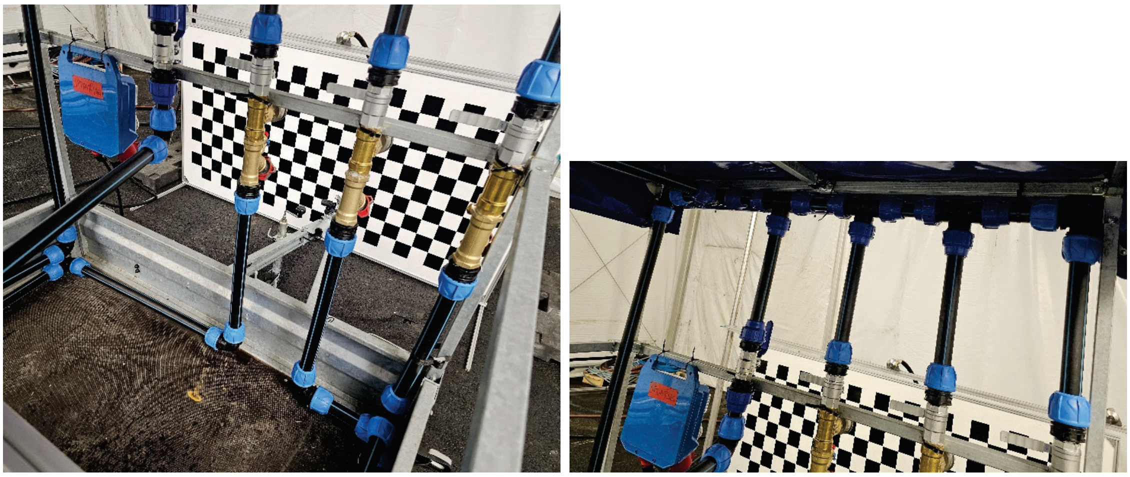

Figure 30 - Pipe installations in the spray rig V2.

Figure 31 - The AstaZero Spray Rig V2 occluding a child pedestrian dummy with severe water spray.

Figure 32 - AstaZero Spray Rig V2 produces water spray in a dynamic test scenario in 50 kph.

9. Dissemination and publications

9.1. Dissemination

How are the project results planned to be used and disseminated?	Mark with X	Comment
Increase knowledge in the field	X	
Be passed on to other advanced technological development projects	X	Will result in a follow-up project in some form. Application process is ongoing
Be passed on to product development projects	X	Further development of the Spray Rig is being done in an internally funded project
Introduced on the market		
Used in investigations / regulatory / licensing / political decisions		

During the length of the project there has been several workshops with the partners in the AI-SEE project to disseminate current results and discuss the project topics further. The project in its whole was also presented during the final event for AI-SEE held at the AstaZero test site the 11-13th of November 2024 and on the SAFER Research Day at Lindholmen Science Park on the 18th of December 2024. From the AI-SEE event a LinkedIn post with short information was published with short movies to spread information outside project partners of AI-SEE and SEVVOS [16].

All evented listed below:

2022 6-7/9 AI-SEE Consortium Meeting in Ingolstadt/CARISSMA

2023 30/8-1/9 AI-SEE Consortium Meeting in Tampere/VTT

2024 16-18/4 AI-SEE Consortium Meeting in Graz/AVL

2024 11-13/11 AI-SEE Final Event/AstaZero

2024 18/12 SAFER Research Day/Lindholmen

9.2. Publications

"Comparing Vehicle Safety Systems in Adverse Splash and Spray Condition between Road and Test Site." – SIAs VISION 2022 Conference [18]

"Characterisation and variabilities of sprays produced by tyres rotating on wet surfaces." - WCX SAE World Congress Experience [19]

10. Conclusions

In the application, work package one was about Project Management and Demonstration. SEVVOS have performed all tasks according to plan. Data set from tests are available at Astazero and could be delivered on request.
Work package two is about identifying spray scenarios in naturalistic conditions and in simulation. Several data collections have been done from naturalistic driving but due to many dynamic changing variables the project has not been able to measure, compare and draw measurable conclusions. Magna's naturalistic data provided insights into adverse weather effects on image quality and contributed to validating AstaZeros spray rig. Chalmers’ simulations showed how water film depth and spray dynamics are influenced by vehicle speed, tyre tread, and water application methods. Spray generation with a 100 μm water film depth was effective, while numerical studies highlighted the need for further research into far-field spray propagation and visibility impacts.
Work package three included spray tests at AstaZero & Rise. The various tests and studies provided valuable insights into visibility degradation caused by water spray and the physical characteristics of aerosols generated by vehicles.
Tape Tests on Multilane Road and High-Speed Area: While not all runs yielded usable data, patterns emerged under controlled conditions. Deeper water depths (9-10 mm) consistently led to greater contrast degradation compared to shallow water (4-5 mm). Increased vehicle speed amplified the effects, with shallower water showing more pronounced contrast changes. Variations in light conditions, particularly between September 16th and 17th, highlighted the influence of external factors.
Indoor Tests with Spray Rig: Dynamic tests encountered challenges with automated contrast analysis due to low resolution and insufficient lighting. However, static tests revealed that higher light levels enabled repeatable contrast degradation patterns, while high-beam headlights significantly increased degradation by illuminating spray particles.
Tyre Rig Spray Tests at RISE: Controlled tests quantified aerosol characteristics, showing that rotational speed and water depth significantly affected droplet size, distribution, and contrast degradation. Higher speeds and reduced water depths increased aerosol density but narrowed the contrast range. Larger water depths resulted in the lowest average contrast values.
Overall, the findings in work packages two and three emphasize the critical role of water depth, speed, lighting, and tyre dynamics in spray generation and visibility degradation. Despite challenges, the results offer a strong foundation for improving experimental methods and mitigating visibility issues in wet conditions.
Work package four was about securing a spray rigg that could emulate water spray in a naturalistic and repeatable way with documented method and possibility to calibrate. This was fully succeeded and proven in test.

11. Future work

As any good project should, we have more questions now to answer than we had before the project started. These questions will be reshaped into future internal projects, project applications or consortia cooperations.

More data needs to be collected on real-world water spray, both regarding contrast attenuation and droplet characteristics. This data can then be used to make the spray created with the spray rig even more realistic.

One key component for this data collection, as we see it, is to measure the water film thickness on the road in front of the tyres. This would remove all the complications to keep a certain determined water depth on the test are when collecting data. If this was solved it would be possible to either collect data on test track or public roads after or during rain or wet the surface in front of the car with a water truck and perform tests at a test track.

Real-world data could also be collected by some stationary setup on a public road. The water film thickness on the road would be monitored continuously. A camera could detect every passing vehicle and classify the model/size of it. Then light extinction and, contrast could be measured for the spray created by the passing vehicle. Some obvious drawbacks would be the complexity in the setup with permissions from authorities, traffic safety and avoiding vandalization. Unfortunately, this would only generate data perpendicular to the driving direction, while data from straight behind the vehicle would be of more relevance.

In all this there is also needs to better define methods and processes to measure contrast while driving behind the spray rig or another vehicle. Future projects also need to find methods that are less sensitive to different light conditions, this is a key to be able to compare data from naturalistic driving with spray emulated with rig. Much focus in this project has been on stationary spray rig.

Throughout both this and the previous project SUS, the goal has been to replace the checkerboard target with any target/object and our Lumix camera with any sensor. The purpose of the checkerboard and camera is to calibrate and determine the current contrast attenuation created by the spray and then combine it with the sensor data from the sensor under test. This needs to be investigated further.

12. Sources and links

1. AI-SEE - https://www.ai-see.eu/project
2. "Tefft, B.C.: *"Motor Vehicle Crashes, Injuries, and Deaths in Relation to Weather Conditions, United States, 2010-2014"*. Technical Report. Washington, D.C.: AAA Foundation for Traffic Safety, 2016."
3. Spray1 (2014-05601) - Spray1 | Vinnova
4. Spray2 (2015-04837) - Spray 2 | Vinnova
5. Weather Generation at AstaZero (2018-01930) - Vädergenerering på AstaZero | Vinnova
6. SUS (2020-02961) - Sensorprovning i Utmanande Siktförhållanden (SUS) | Vinnova
7. Adose - https://www.researchgate.net/publication/299712739_Enhanced_Low-Cost_Sensing_Technologies_for_Vehicle_On-Board_Safety_Applications_ADOSE_Project
8. PReVENT - https://cordis.europa.eu/article/id/85526-on-the-road-to-reducing-accidents
9. HAVEit - https://cordis.europa.eu/project/id/212154
10. MiniFaros - https://cordis.europa.eu/project/id/248123/de
11. Artrac - https://tutech.de/artrac/
12. AdaptIVe - https://www.adaptive-ip.eu/
13. RobustSENSE - https://www.robustsense.eu/
14. DENSE - https://www.dense247.eu/
15. *Physical characteristics of spray clouds produced by heavy vehicles (trucks and lorries) driven on wet asphalt* - https://ri.diva-portal.org/smash/record.jsf?faces-redirect=true&aq2=%5B%5B%5D%5D&af=%5B%5D&searchType=SIMPLE&sortOrder2=title_sort_asc&query=&language=sv&pid=diva2%3A1588836&aq=%5B%5B%5D%5D&sf=all&aqe=%5B%5D&sortOrder=author_sort_asc&onlyFullText=false&noOfRows=50&dswid=7555
16. Spray nozzles supplied from *https://www.pnrnordic.se/*
17. *LinkIn post about the AI-SEE Final Event - https://www.linkedin.com/posts/automotive-at-rise_astazero-adasmanagementconsulting-ilm-activity-7264592884014743552-3Ojz?utm_source=social_share_sheet&utm_medium=member_desktop_web*
18. *Comparing Vehicle Safety Systems in Adverse Splash and Spray Condition between Road and Test Site* **-** https://www.saferresearch.com/library/comparing-vehicle-safety-systems-adverse-condition-splash-and-spray-between-road-and-test
19. *Characterisation and variabilities of sprays produced by tyres rotating on wet surfaces* **-** https://www.sae.org/publications/technical-papers/content/2025-01-8763/

13. Participating parties and contact persons

Mari Eriksson – AstaZero – mari.eriksson@ri.se
Peter Eriksson – AstaZero – peter.n.eriksson@ri.se
Jan-Erik Källhammer – Magna - jan-erik.kallhammer@magna.com
Paul Otxoterena – RISE - paul.otxoterena@ri.se
Valery Chernoray – Chalmers - valery.chernoray@chalmers.se

14. Appendix A – Magna Report

SEVVOS – a FFI project

WP 2 Collection of field data under adverse weather conditions

2024-12-06

Table of Contents

Summary of the Project

Perception systems in current serial vehicles were designed for fair weather conditions, resulting in degraded performance in adverse visibility conditions such as fog, snow, rain, or spray from vehicles ahead. Addressing this shortcoming brings challenges in the development and validation of such systems. Consistent adverse conditions are quite rare, imposing a challenge to collect sufficient relevant data to validate the system. A key difficulty in adverse conditions testing is therefore the lack of repeatability. Tests done at different instances in time and location are difficult to compare and measures of variability essential to consider when assessing differences.

Our project aims to map the conditions for testing perception systems under the influence of adverse weather conditions. The primary objective for the work is to evaluate different kind of sensor and camera technologies at an early stage and under real-world conditions. This kind of early evaluations can help us to make decisions about future product capabilities. It is also possible to invite customers for technology test drives strengthening existing or creating new relationships.

Scope, Work package 2

Work package 2 involves the collection of field data under naturalistic conditions. The goal is to create an understanding of how aerosols and spray are created for different vehicle combinations and in different traffic situations. This will then be used to be able to recreate spray scenarios in simulation that are difficult for optical perception systems in vehicles. The result is in the form of a database of video sequences. The data is mainly expected to provide valuable insight into how a static and dynamic spray simulator can be built at AstaZero.
Magna can install up to nine different camera sensors and a lidar in a test vehicle, which is intended to be collected in connection with the associated PENTA-EURIPIDES[2] co-labelled project AI-SEE. A subset of data will be shared to all SEVVOS project members for analysis of spray from normal driving.

Approach

Consistent adverse conditions are rare, imposing a challenge to collect sufficient relevant data to validate the system. Hence, a key difficulty in adverse conditions testing is the lack **of comparable and repeatable conditions**. For testing in adverse weather, naturalistic field tests are of course the ultimate reference, but tests done at different instances in time and location are difficult to compare. This leads to that it is hard to assess system performance changes when the variabilities in test conditions may be larger than the expected system performance changes.

So, how do we then achieve comparable and repeatable tests when conditions under naturalistic field tests made at different points in time are not consistent over time? Since **comparable** naturalistic tests are hard to achieve, we instead focus on recording different relevant, or potentially relevant sensors simultaneously, to at least ensure that the environmental exposure to the different sensors was uniform in the particular instance in time. Here we disregard the minor variability caused by the fact that the different sensors are not mono-statically mounted but spread across the width of the vehicle, at an elevated position on the roof of the vehicle.

We implement this approach by equipping the test vehicle with all considered cameras and record simultaneously to allow uniform conditions for all involved cameras. We therefore built a test vehicle with a distributed sensor data collection system that can be expanded with more PC's if bandwidth or CPU/GPU limitations is reached. An internal software plugin architecture makes the system easy to adapt to new sensors, new interfaces, and new processing technologies. The graphical user interface is designed for simplicity, allowing it to be easily used by the driver without undue distraction.

During post-drive sensor data evaluation, the full resolution and framerate of the sensors is available for further analysis. The data collection software has been deployed in a Mercedes S-class, currently equipped with seven different cameras/sensors.

Figure 1 shows the exterior of test vehicle with the sensors integrated in a roof mounted canopy where glass without IR blocking filters more easily could be implemented. The images of the various sensors are shown on the graphical user interface to the driver.

Figure 1 Test vehicle with unit under test and reference sensors mounted in a canopy on the roof and the driver's graphical interface.

Figure 2 shows an example of the recorded sensors.

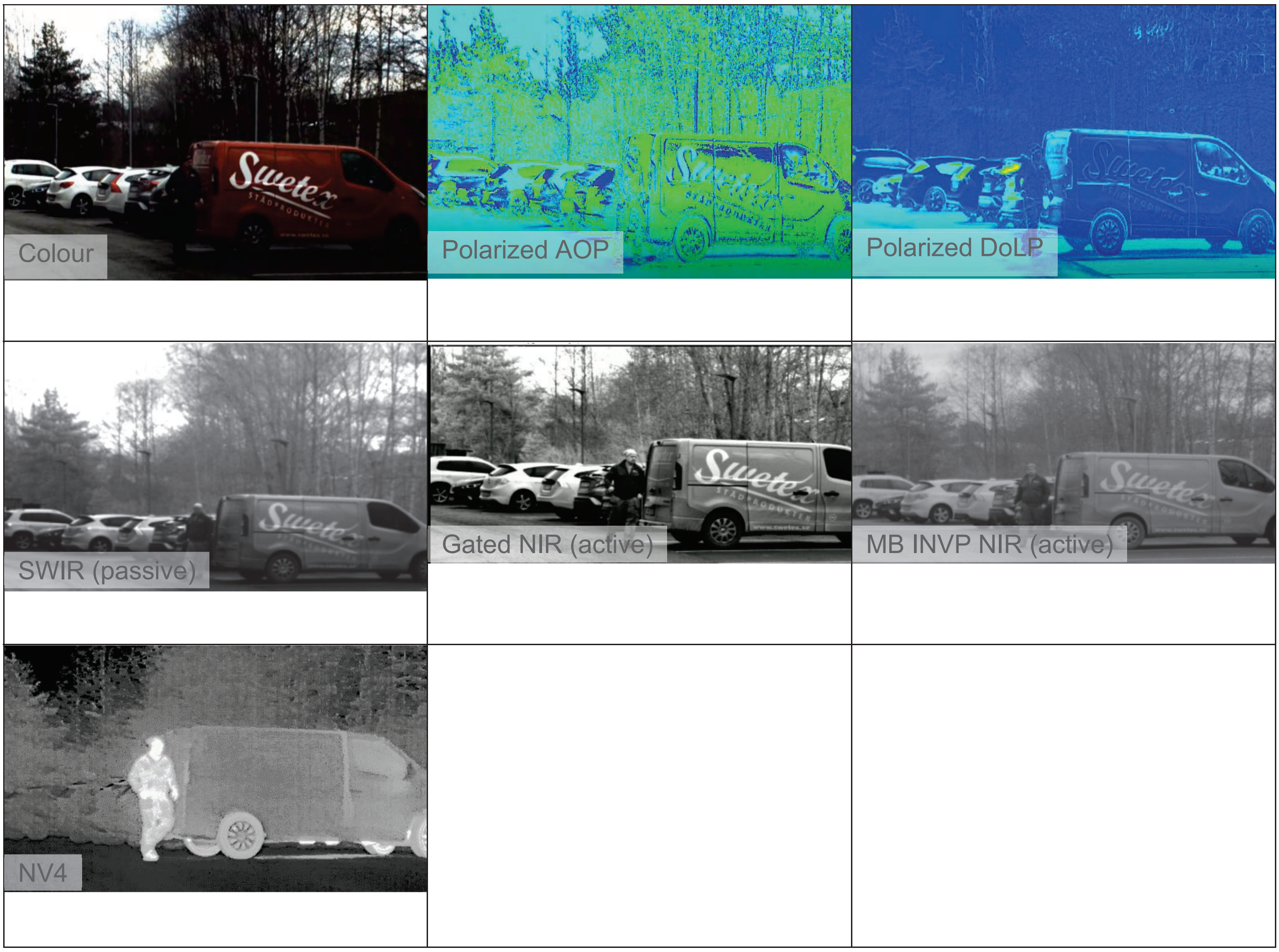

Figure 2 Example collected images.

As **repeatable** tests are hard to achieve in naturalistic settings, we also focused on developing **repeatable** tests under controlled circumstances to not just reduce variabilities in the tests but also greatly reduce the costs and time duration of testing due to the varying availability of suitable weather and other ambient conditions. Together with AstaZero we focused on developing a test rig for spray. Spray brings challenges in the development and validation of perception systems. Spray is caused by vehicles traveling on wet surfaces. Aerosols and spray in the form of splash and spray clouds are produced. These water droplets have a significant impact on vehicle soiling, visibility, and the operational capabilities of sensors used in driving assistance systems and future autonomous vehicles.

For assessing the spray generation rig vs naturalistic conditions, we investigate the effect on the image quality in different wavelength and camera types. The same parallel sensor acquisition setup used to compare naturalistic conditions can therefore also be used when developing more repeatable test methods. If the various sensor outputs in naturalistic driving are similar across the sensors with different wavelengths as compared with our developed test method, we can assume that the spray characteristics are similar with regards to the main criteria of droplet size and droplet count.

SAE J2245[1] is a recommended practice for splash and spray evaluation. It describes two methods of analysis, by either measuring light extinction or by contrast measurements. We use SAE J2245 as a guide to assess levels of spray in various situations and focus on the contrast measurements as cameras are one of the main sensors used for driving automation. Quantifications are done either by means of laser methods for light extinction or video digitizing for contrast measurements.

SAE J2245 uses a figure of merit, FOM defined as:

$$FOM = \frac{Cc - Ct}{Cc} * 100$$

where Cc is the contrast in the **control** image at each location
Ct is the contrast in the **test** image at each location

This is calculated for each location of the checkerboard. The share of the checkerboard that is obscured is then averaged. This means that corresponding locations are important. In a situation with dynamic spray and somewhat varying positions due to vehicle movement and non-fixed distances to the vehicle carrying the contrast target, we instead opted to use Michelson[2] contrast:

$$C = \frac{Cmax - Cmin}{Cmax + Cmin} * 100$$

where Cmax is the max intensity in the image at measured location
Cmin is the min intensity in the image at measured location

The max. intensity corresponds to the white part of the contrast target while the min. intensity corresponds to the black part of the contrast target (in our case the checkerboard).

An example is given in Figure 3. Here the white areas are around 180 while the black areas are around 70, generating a contrast at around 44%. The measurement accuracy will benefit if the image base (unaffected) conditions is stretched to the full dynamic range of intensities, but it also means that the same camera settings will be needed for the degraded images. Care is needed not to saturate or bottom-out the camera in any of the sensing locations.

This measure can be applied in different ways, either on each transition (edge of each square), on the average of each black/white square, or on average for the whole checkerboard, depending on what focus we place on the analysis. The right pane in Figure 3 illustrates that the contrast measure will be slightly higher using the transition at the edges vs. using the average intensities in each black and white square. The higher contrast at the edges can in some cases be an artifact of edge enhancement features in the camera or recording system. An average contrast can either be calculated as an average of contrast of each black/white transition or square averages, or calculated using histograms as illustrated in Figure 4 and Figure 5.

[1] SAE International: *"J2245 Recommended Practice for Splash and Spray Evaluation*". Warrendale, PA., 2011.
[2] Michelson, A. (1927). *Studies in Optics*. U. of Chicago Press

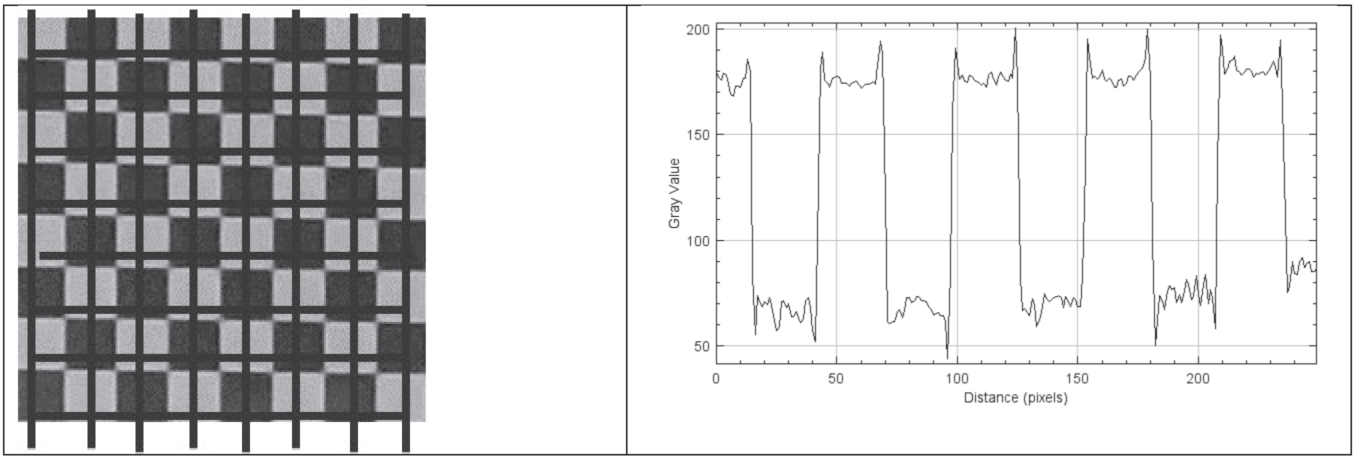

Figure 3 Contrast measurement over each white/black transition (left), with example intensity variations (right)

Figure 4 shows an example of spray from a car ahead on a wet road. The left panes show images with a checkerboard contrast target mounted behind a vehicle at two different speeds. Under equal ambient conditions the spray generally increases with high speed, hence the resulting contrast diminish. The right panes show the resulting histogram of the checkerboard contrast target. Higher contrast produces two distinct peaks with larger separation.

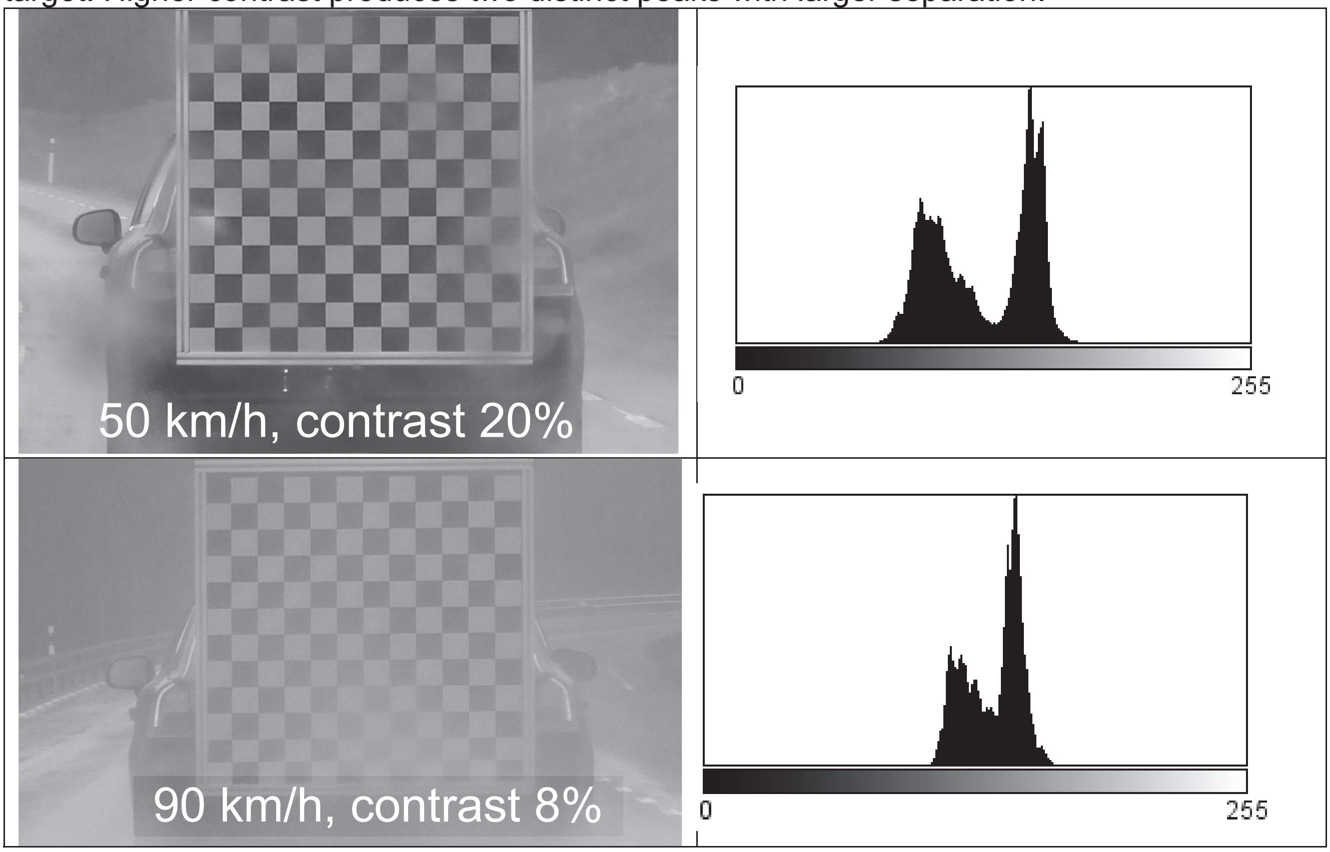

Figure 4 Global contrast measurements using histogram method when driving on wet road.

Figure 5 shows an example of contrast degradation from artificially generated spray. Similar as in Figure 4, the left panes show images with a checkerboard contrast target and the right panes show the resulting histogram of the checkerboard contrast target. With very low contrast the two peaks have almost merged completely.

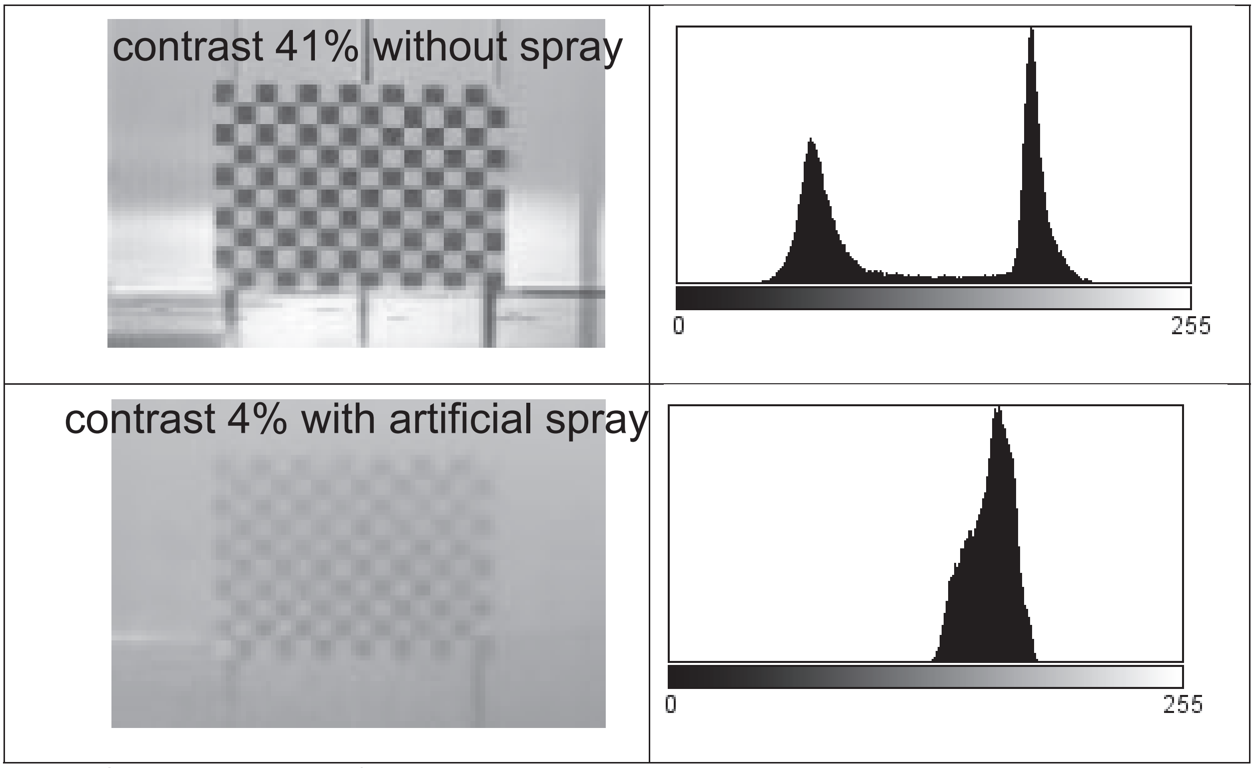

Figure 5 Contrast measure in artificially generated spray.

Comparing the resulting contrast degradation from the spray generating rig coincide with a visual perception of the amount of contrast degradation in naturalistic situations.

Data collection events

There have been four main data collection events. The amount of data is given after each event. In total it encompasses a total of 341 GB of data.

1. Winter tests, Muonio, Finland, 14-17 Feb 2023 213 GB
2. Spray on wet road, Vårgårda 8 Aug 2023 24 GB
3. Off-road, Padasjoki, Finland, 29-30 Aug 2023 82 GB
4. Artificial spray, AstaZero Dryzone 17 June 2024 22 GB

Winter tests

These tests were collected in cooperation with VTT Technical Research Centre of Finland, benefitting from the association with the PENTA project AI-SEE. The behavior of snow depends on the characteristics of snow. Wet snow (slush) that freeze can accumulate on vehicle surfaces – including sensor locations – to completely block the view of the sensor, as illustrated in Figure 6.

Figure 6 Wet snow that freeze may block sensors

In contrast, a vehicle moving on a road with dry snow generate a cloud of snow with an effect similar to the spray cloud generated by a vehicle moving on a wet road. An example can be seen in Figure 7.In the lower pane the contrast is degraded to the point that it is hard to even distinguish the presence of the contrast checkerboard.

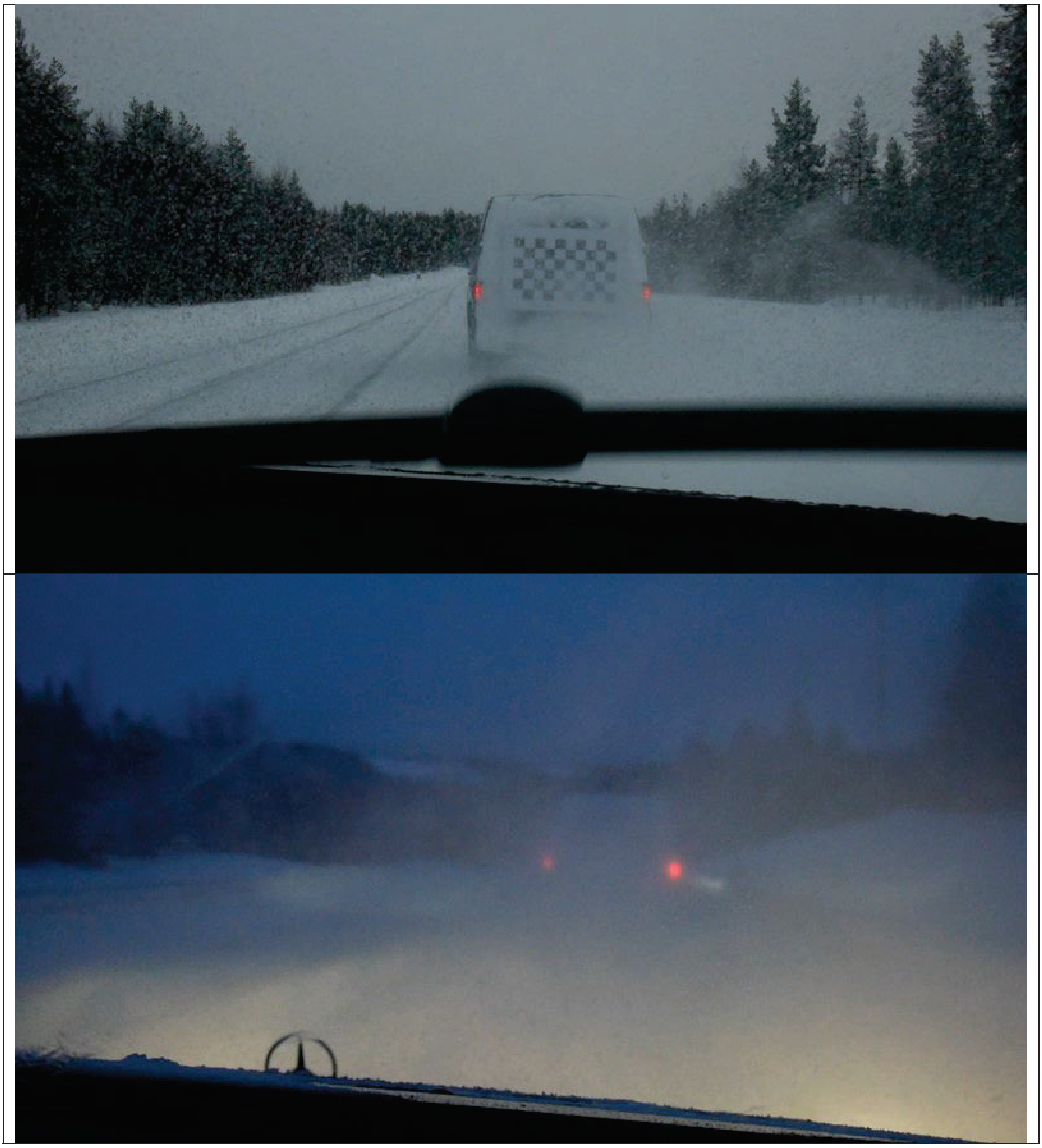

Figure 7 Example of the effect of snow on image contrast.

Spray tests on wet road

The data collection on a wet road was done on the newly built motorway between Vårgårda and Alingsås. It was conducted in late summer with rather heavy rain reported at 2 mm/hr. The newly completed stretch of road was chosen to have as uniform amount of water on the road, hence avoiding the recesses in the main wheel tracks created in a worn road. Even so, the amount of spray very a lot as seen in Figure 8. The two images are captured only a few seconds apart.

Figure 8 Example of the effect on image contrast from spray generated by a vehicle travelling on a wet road.

Some of the degraded image is caused by the scatter of light in the area between the vehicles, and some of the image degradation is caused by the water film on the glass (windshield) that builds up between each stoke of the windshield wipers. The large variability emphasizes the need for more controlled and repetitive test methods which is a main focus of this project.

Off-road

These tests were collected in cooperation with VTT Technical Research Centre of Finland, benefitting from the association with the PENTA project AI-SEE. They were collected on a military proving ground near Padasjoki, Finland. Recent rain limited the amount of dust and instead emphasized mud and dirt as the cause of image degradation.

Artificial spray

These tests were collected in the AstaZero Dryzone using the AstaZero developed spray-rig. The location in the Dryzone allowed operation without disturbances from wind or sun on the generated spray. Wind causes the spray to dissipate while sun generated disturbing light scatter.

Figure 9 Example of the effect on image contrast from artificially generated spray.

Conclusion

A selection of adverse weather conditions under naturalistic conditions have been collected at a spectrum of conditions that may be encountered by a vehicle. It has generated an understanding of how obscurants in the atmosphere affect the captured image quality of on-board cameras and other sensors.
It has generated a database of image sequences that are available to all project partners.

The data has been instrumental to generate the reference to which the AstaZero developed spray-rig is compared.

Some of the data collection events has greatly benefitted from the cooperation with VTT Technical Research Centre of Finland, benefitting from the association with the PENTA project AI-SEE.

Forward.
For all.

15. Appendix B – Chalmers Report

Splash and Spray Measurement and Simulations

Valery Chernoray [1]

[1] Dept. of Mechanics and Maritime Sciences, Chalmers University of Technology, 41296 Gothenburg, Sweden

***** Correspondence: valery.chernoray@chalmers.se

Abstract: For enabling reliable automated vehicles that work in all weather conditions, it is crucial for vehicle and sensor manufacturers to have access to test environments, both physical and virtual, that simulate adverse road conditions. This study reviews previous works and describes methods for numerical simulations of water spray developed at Chalmers under the Vinnova-funded project SEVVOS. The research is fundamental for the development and testing of sensor systems for operation in severe weather, and therefore it is essential for the vision of zero road accidents, with particular focus on self-driving vehicles and driver assistance systems.

Keywords: Rain; Wet Road; Vehicle; Splash and Spray

---

1. Introduction

A vehicle rolling on a wet road generates a cloud of water spray around it, which obstructs visibility and causes contamination for both the vehicle itself and for other road users. Water spray is characterized by the spatial distribution of droplets, droplet size, and concentration. All these spray parameters are dependent on the vehicle's speed and geometry, its tires, road surface, weather conditions (e.g., water depth on the road, precipitation, wind), driving environment (e.g. city, countryside, bridge, tunnel), and road situation (e.g. driving behind, overtaking). The development of a relevant and repeatable physical test environment is impossible without a clear understanding of the crucial aspects to include in the test environment and how to model these aspects. To create a representative and repeatable artificial spray, it is essential to know the parameters of a real spray. Since the total number of parameters involved is too large for experimental studies, a test matrix can be reduced with the help of a review of previous studies and theoretical and numerical modelling.

Weir et al. (1978), Clarke (1983), and Pilkington (1990) explain differences between splash and spray. Splash is composed of water jets, ligaments, and large drops (larger than 1 mm) that travel primarily in low trajectories close to the ground, although some can be ejected high. Spray is composed of a fine aerosol mist (less than 0.5 mm) primarily created after droplet breakup (atomization) due to interactions with each other, the airflow, and solid surfaces. The splash is quickly returned to the ground while the spray cloud remains suspended in the air, surrounds the vehicle, and stays at a large distance behind the vehicle causing a considerable reduction in visibility. Spray is considered the greatest vision-obscuring component. However, splash poses more challenging for lidar systems, which are more severely obstructed by splash than by spray (see e.g. Yoneda et al. 2019, Figure 1).

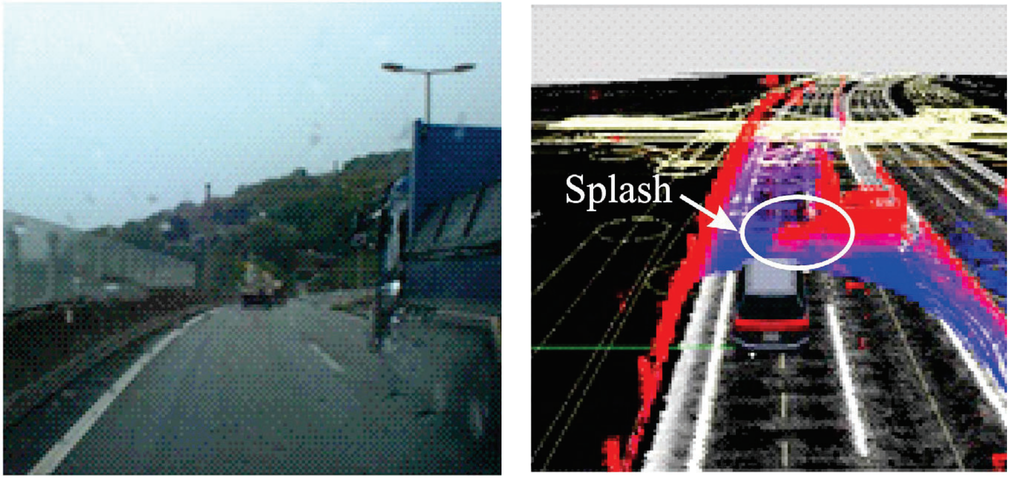

(a) Camera Image **(b)** Lidar Observation

Figure 1. Splash from a heavy vehicle at overtaking. (a) Observed by a camera; (b) Observed by a Lidar. A caption on a single line should be centered. Reproduced from Yoneda et al. (2019).

2. Previous Studies

2.1. Water film depth

The water film depth (WFD) is one of the main factors affecting the generation of splash and spray.

The water film depth is a function of pavement roughness, drainage capability, and rainfall intensity. Anderson et al. (1998) suggest several mathematical models for predicting water film depth. The most recognized model is:

$$w_d = \left(\frac{n \times L \times i}{36.1 \times S^{0.5}}\right)^{0.6} \tag{1}$$

where n is the Manning's roughness coefficient, L and S are the length and slope of the drainage path, respectively, and i is the rainfall intensity. If the pavement's configuration is fixed, the water film depth is fully defined by the rainfall intensity. Several different versions of this equation are available, e.g., in Flintsch et al. (2014) and Yu and Sun (2018), which are very similar to Equation (1) but involve different powers for different terms. **This means that a calibration function between the rainfall intensity and water film depth for a given pavement can be experimentally determined** in the form $WFT = Ai^n$ where A and n are pavement calibration constants with n typically between 0.35 and 0.8.

It is crucial to understand that the undisturbed water film thickness is only encountered by frontal vehicle wheels. The rear wheels travel through a reduced water film while also receiving water in the form of splash and spray from the frontal wheels.

The maximum amount of water in m^3/s which can be picked up by a vehicle from the wet road is:

$$\dot{V} = w_d \times V_0 \times W \tag{2}$$

where V_0 is the vehicle speed, and W is the total width of the vehicle's tires (so-called projected width, as seen from the vehicle front). **This equation predicts the maximum total**

volume of water that can be transformed into a splash and spray. However, the proportion between the volumes of splash and spray is much more complicated to estimate since it also depends on the vehicle speed, tire geometry, vehicle geometry, and wind conditions.

As an example, for a car with a tire width of 2×250 mm moving at 80 km/h (22.2 m/s) on a road with 0.5 mm water film, the total maximum volume flow of splash and spray will be 0.0005*22.2*0.5 = 5.6 l/s. Thus, a system which creates artificial splash and spray will need an estimated maximum capacity of 78 l of water to provide 14 s of testing time sufficient for driving 300 m distance. To irrigate a 300 m long and 5 m wide lane with 0.5 mm water film will require at least the water volume of 300*5*0.0005 = 750 l not accounting for runoff, which would require constant refilling. According to SAE J2245 (2011), the refilling would require up to 190 l/min or 44 l in 14 s, thus giving the total volume of 800 l, which is 10 times more than for a spray system.

2.2. Mechanisms of splash and spray generation

The total volume of splash and spray generated by a vehicle can be defined using Equation (2). The ratio between splash and spray is not simply defined and depends on factors such as water film depth, vehicle speed, tire geometry (inflation/load, tread design, condition), vehicle geometry (aerodynamics, spray suppression devices) and wind conditions (direction, strength), as pointed out by, e.g., Resendez et al. (2007). Typical photographs showing different types of splash and spray generated by vehicles are included in Appendices 1 and 2 of this report.

Weir et al. (1978) proposed four main mechanisms for splash and spray generation by a tire (see Figure 2): bow and side splash waves, tread pickup, and capillary adhesion. Bow and side waves primarily result in splashes of large droplets that follow low trajectories close to the ground and tend to quickly fall back to the road surface. High-intensity bow and side waves are generated when a vehicle moves through a thick water film. Very weak and barely visible bow and side waves are generated when a vehicle moves at high speed on a well-drained road with a thin water film (e.g. a highway), as seen in Appendices 1 and 2. Some parts of the bow and side waves can be atomized after hitting solid surfaces and interacting with air streams. However, tread pickup and capillary adhesion are the primary contributors to spray generation.

Tread pickup consists of droplets collected in tread grooves that are thrown off near the road. These droplets enter the air streams around the vehicle and collide with solid surfaces (e.g., fuel tanks, underbody, spray suppression devices, back wheels), leading to their breakup, atomization, and spray generation. Some droplets stick to solid surfaces, while others return to the ground. **Capillary adhesion spray is generated from a thin water film (about 0.1 mm)** present on a wet tire, which is thrown off later in the rotation than tread pickup, resulting in its release higher above the ground. Most of the capillary adhesion spray hits the wheel housing, where it either sticks or atomizes (see Figure 3). The droplet formation process from a capillary-adhered water film is shown in Figure 4. The process involves the formation of thin ligaments that split into droplets. Capillary adhesion generates droplets ranging from 0 to 0.5 mm in size, while tread pickup generates large water filaments and droplets up to 5 mm in size. According to Weir et al. (1978) roughly 99% of the water picked up by treads is thrown off near the road as tread pickup, with the remaining 1% contributing to capillary adhesion spray**.** Both large and small droplets follow ballistic trajectories when leaving a tire; however, most large droplets quickly return to the ground, while small droplets remain suspended in the air and carried by airflow.

Weir et al. (1978) concluded that for water depths less than about 3·mm, both the water film thickness and tread design influence the amount of water picked up by the grooves and thrown off as tread pickup. As groove volume increases, more water passes through the grooves, and less is displaced in bow and side waves. For water depths greater than 3 mm, the grooves become filled, and excess water in the tire's path is displaced in waves. In this case, the amount of tread pickup becomes independent of the water film thickness. For slick tires, water is thrown similarly to tread pickup but is ejected much nearer to the tire's sidewalls than its center. Tread groove volume and water film thickness are key parameters affecting the ratio of splash to spray from a single wheel. When the wheel is a part of a vehicle, the vehicle's underbody geometry and airflow beneath the body become additional crucial factors.

The rate at which a droplet falls to the ground is characterized by its terminal velocity, also known as settling velocity, which strongly depends on the droplet diameter. For a 5-mm droplet, the terminal velocity is 9 m/s; for a 0.5-mm droplet is 2 m/s; for a 0.2-mm droplet is 0.7 m/s; and for a 70-µm droplet, it is 0.15 m/s (see, e.g., Best 1950). A droplet's ability to follow airflow is characterized by its Stokes number (see, e.g., definitions in Kabanovs et al. 2019 and Hagemeier et al. 2011). The Stokes number characterises the droplet's inertia and how well it follows the motion of an accelerated flow. Smaller terminal velocities and Stokes numbers indicate better flow following and slower settling. Thus, particles of different sizes follow significantly different paths in the airflow.

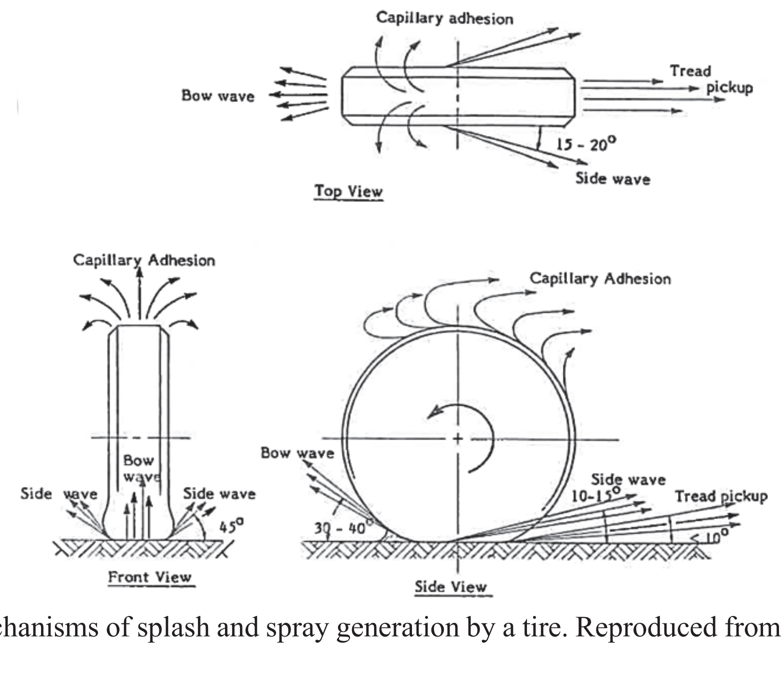

Figure 2. Mechanisms of splash and spray generation by a tire. Reproduced from Weir et al. (1978).

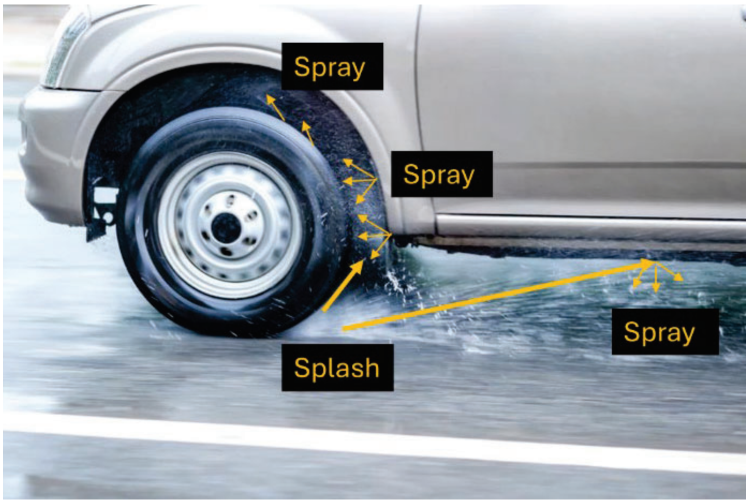

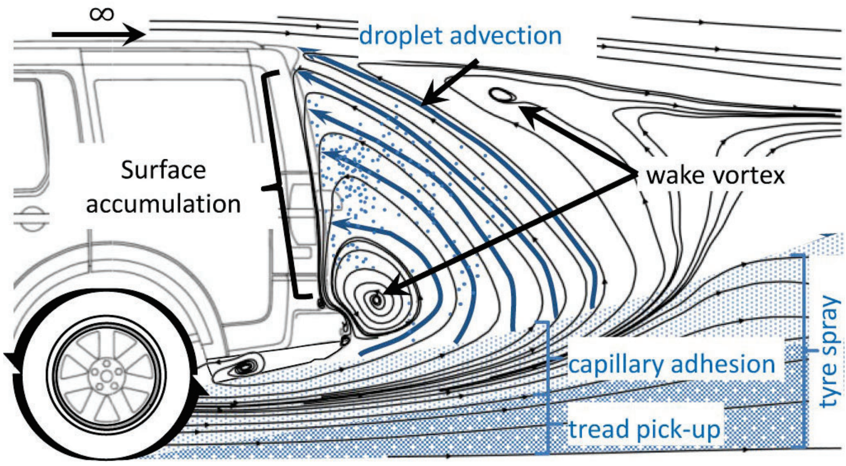

Figure 3. (Top) Splash and spray generation by a tire. (Bottom) Splash and spray propagation behind a vehicle. Reproduced from Jilesen et al. (2017).

Weir et al. (1978) also provide guidelines for spray cloud estimations. The length of the spray cloud trailing a vehicle is proportional to the square of the vehicle's velocity. The spray density within the spray cloud increases approximately with the cube of the vehicle's velocity (see also Flintsch et al. 2014). Since the amount of water encountered by an adjacent vehicle equals the spray density multiplied by the vehicle's velocity, the visibility effect increases approximately with the fourth power of the velocity.

The theory of splash and spray by Weir et al. (1978) was successfully applied by Clarke (1983) in designing spray suppression devices for heavy vehicles.

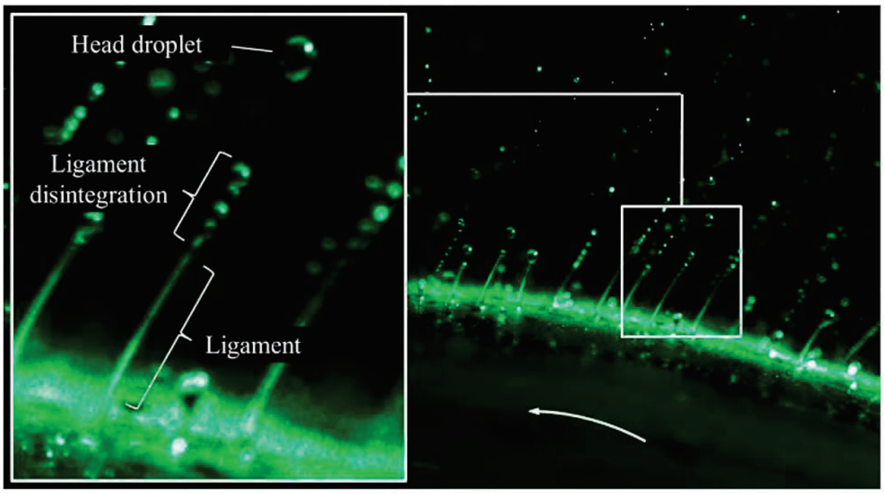

Figure 4. Spray generation from a capillary adhered water film on a tire top. Reproduced from Strohbücker et al. (2019).

2.3. Measured droplet size distributions

2.3.1. Droplet size distribution near a single wheel

Strohbücker et al. (2019) present measurements of a droplet field around a single rotating tire in a wind tunnel. The droplet field is illuminated by a laser plane and the droplet size and droplet velocity for two different tread designs and tire speeds are evaluated. Slick and grooved kart tires with an outer diameter of 251 mm were used. **The tires rolled on a 0.1 mm thick water film** and were exposed to airflow at 20 km/h. Figure 5 shows the droplet diameter distribution and the droplet velocity near the tires. The mean droplet diameter was calculated from the total mass and total number of particles presented in Figure 16 of Strohbücker et al. (2019) and represents a mass-averaged mean diameter. The definition of the circumferential angle is also shown in Figure 5 and is consistent with the definition in Kabanovs et al. (2019).

As seen from Figure 5, the mean droplet diameter remains constant for both tires at 40 km/h and is about 0.4 mm, except for the 0-degree position on the grooved tire, where the diameter increases to 0.5 mm. At 120 km/h, the mean diameter distributions are nearly identical for both tires and thus appear independent of the tire tread. This observation can be explained by the thin 0.1 mm water film used in the study. The diameter gradually increases for angular positions between –20 and 80 degrees and remains approximately constant (0.28 mm) near the tire top, at angular positions 80 to 160 degrees. The circumferential variation of the droplet size aligns with the droplet formation physics illustrated in Figure 4. The water film on the tire becomes thinner with increasing circumferential position. A thinner water film results in thinner detached water filaments, which break up into smaller droplets. The same phenomenon occurs when the tire velocity increases—the water film and the filaments become thinner, and the droplets become smaller. Kabanovs et al. (2019) applied a boundary condition for the droplet size distribution on a tire based on this physics.

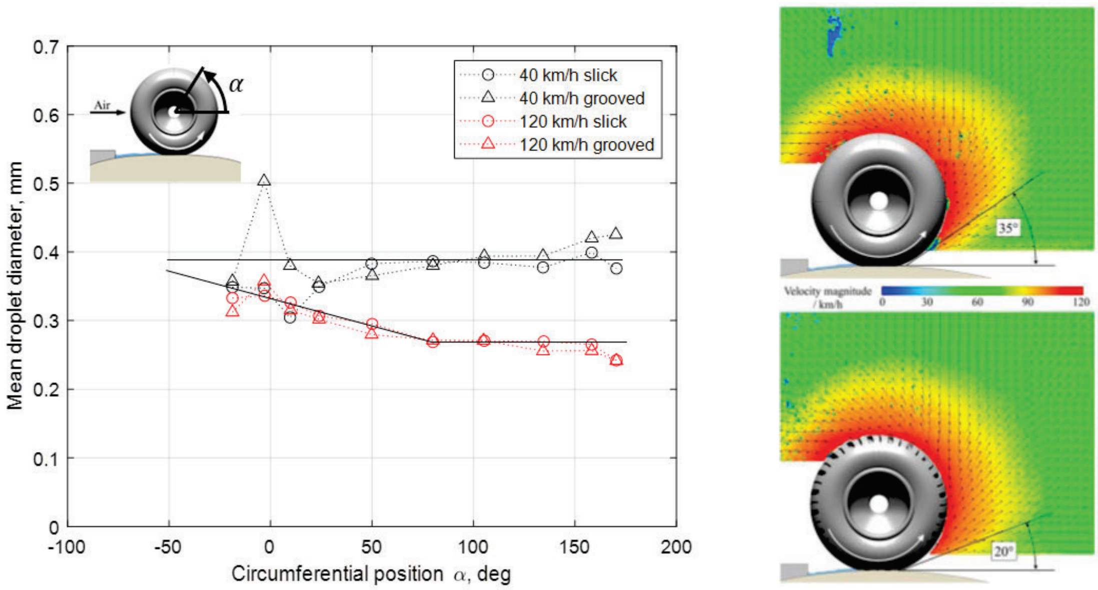

(a) **(b)**

Figure 5. (a) Mean droplet diameter distributions near a slick and grooved tire at 40 and 120 km/h. Based on Strohbücker et al. (2019) data. (b) Droplet velocity field near a slick tire (top) and grooved tire (bottom) at 120 km/h. Reproduced from Strohbücker et al. (2019).

Strohbücker et al. (2019) did not find any pronounced influence of the tire grooves on the particle size. Even in a zone close to the contact patch, the particle size distributions were similar for both slick and grooved tires. This is most likely due to the small thickness of the water film (0.1 mm) used in the experiments. With such a small film thickness, the capillary adhesion was the dominant mechanism for spray formation, making the grooves insignificant. This observation also aligns with the theory proposed by Weir et al. (1978).

Nevertheless, Strohbücker et al. (2019) noted that the water throw-up velocity near the ground was greater for the grooved tire than for the slick tire, as shown in see Figure 5, right. The reason for this is that near the ground, the droplets are formed as a result of the stretching of water filaments between the tire and the ground. The droplets formed by this stretching have lower velocity than the tire. For the slick tire, this was the only mechanism of droplet formation. However, for the grooved tire, there was an additional population of droplets formed between the grooves. These droplets were ejected with a higher velocity (equal to the tire velocity) and contributed to the increased droplet velocity near the contact patch.

2.3.2. Droplet size distribution near a vehicle

Bouchet et al. (2004) performed wind tunnel measurements of the droplet size distribution in a spray near a vehicle. Water was injected in front of the rear wheel as illustrated in Figure 6. Particle distributions were measured 1 meter behind the rear wheel. At a vehicle speed of 80 km/h, the mode droplet diameter was 0.2 mm (Figure 6) and the mass-averaged mean diameter was 0.23 mm. An increased tire speed resulted in a decreased mode diameter and an increased percentage of small droplets in the population. The mode diameter reduced to 0.18 mm at 140 km/h, and the mass-averaged mean diameter reduced to 0.21 mm.

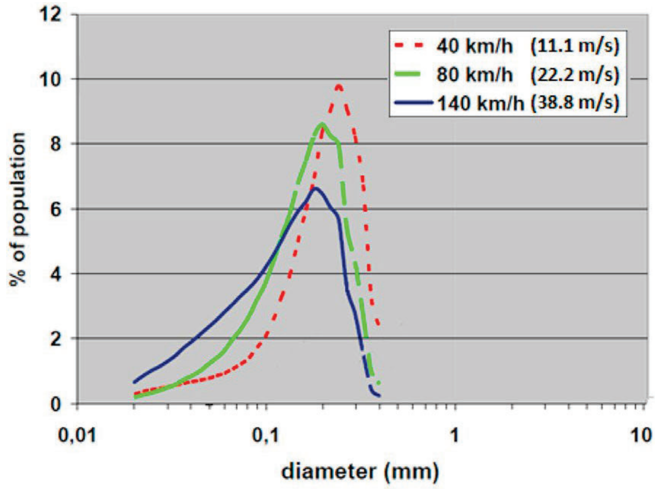

(a) (b)

Figure 6. (a) Wind tunnel set up and (b) spray droplet size distributions at 1 m behind rear wheels. Reproduced from Bouchet et al. (2004).

The diameter reduction with the tire speed aligns with the physics of water film breakup. At higher speeds, the thickness of the water film on the tire decreases, and the ejected water filaments also become thinner; consequently, droplets detached from the filaments are smaller, see Figure 4. **The mean droplet diameter (0.21-0.23 mm) correlates closely with the droplet diameter measured near the tire by Strohbücker et al. (2019) and is slightly smaller, as expected, at a larger distance from the wheel.**

2.3.3. Droplet size distribution far from a vehicle

Shearman et al. (1998) and Borg and Vevang (2006) provided measured droplet size distributions in a spray far behind a vehicle. These results can be found in a review by Gaylard et al. (2017). Shearman et al. (1998) performed PDA measurements on a spray generated by a lorry travelling at 97 km/h on a wetted test lane. The distribution (Figure 7) was dominated by droplets with diameters less than 0.1 mm and featured two peaks: a large peak at the smallest measured diameter (9 µm) and a secondary peak at 0.07 mm. The number-averaged particle diameter was 0.09 mm.

Borg and Vevang (2006) used hydrophobic plates to measure spray droplets in a wake behind a truck driving on a wetted test lane. Their results (Figure 8) show that the distributions peaked at the mode diameter of 0.06 mm both 25 m and 50 m behind the truck. The distributions had number-averaged mean diameters of 0.075 and 0.07 mm at 25 m and 50 m, respectively.

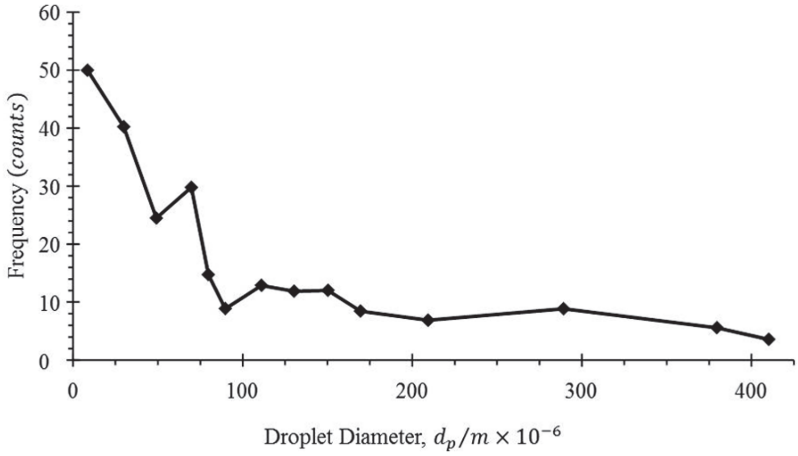

Figure 7. Droplet size distributions behind a lorry at 97 km/h measured by Shearman et al. (1998). Reproduced from Gaylard et al. (2017).

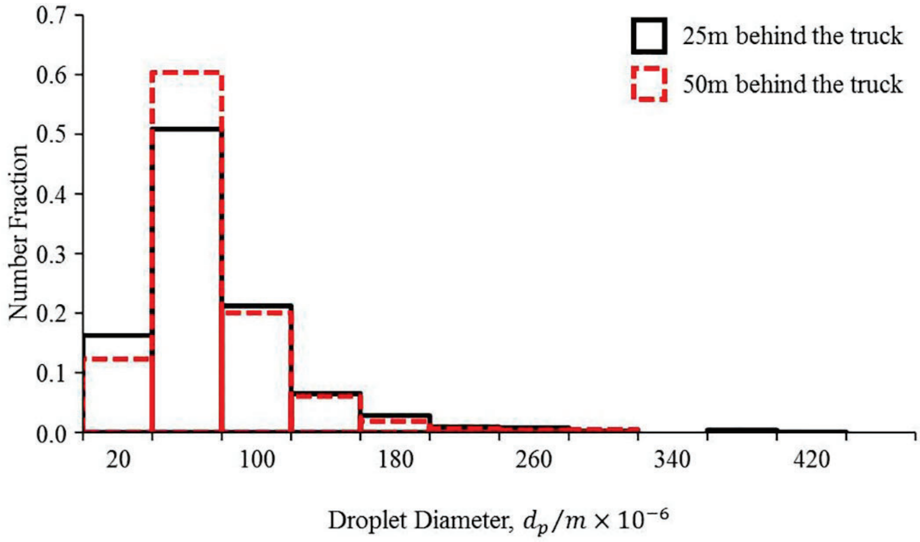

Figure 8. Droplet size distributions behind a truck measured by Borg and Vevang (2006). Reproduced from Gaylard et al. (2017).

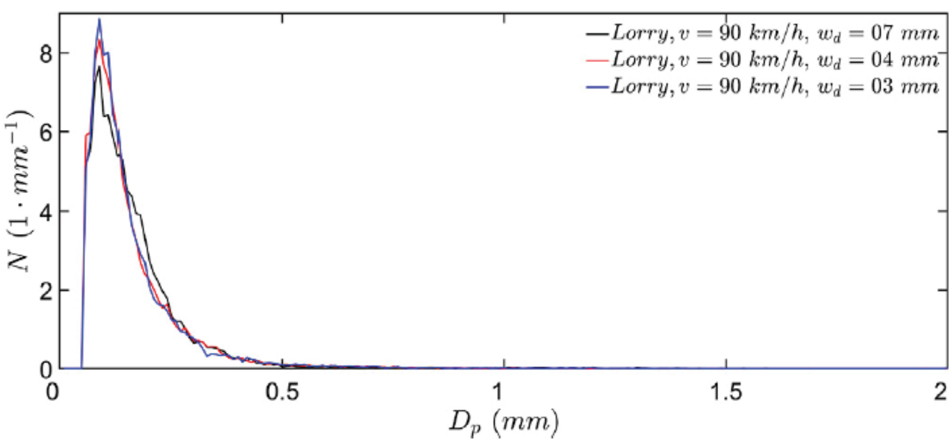

Figure 9. Droplet size distributions after passage of a lorry at 90 km/h at water film depths of 7, 4 and 3 mm. Reproduced from Otxoterena Af Drake et al. (2021).

Otxoterena Af Drake et al. (2021) used shadowgraphy to measure spray distributions from a passing truck on a wetted lane at the AstaZero's test track. The lane was irrigated and surrounded by a barrier to maintain a constant water film thickness. Measurements were collected 0.8 m from the passing vehicle at a height 0.6 m above the ground. Droplet distributions for a lorry driving at 90 km/h on water depths of 7, 4, and 3 mm are presented in Figure 6. The distributions peaked at approximately 0.09 mm and the mean diameter is approximately 0.15 mm. The paper also provided data of the maximum droplet size, number density, mass concentration, light extinction, and contrast. The authors concluded that reducing the water depth produced slightly narrower droplet size distributions with higher fractions of small droplets, whereas increasing the water depth led to slightly wider distributions with higher fractions of large droplets.

The results in this section show that the droplet diameter in a spray far from a vehicle has a mean value of 0.07-0.15 mm compared to 0.2-0.23 mm near a vehicle. This difference can be explained by the larger droplets settling more quickly and returning to the ground, while smaller droplets remaining suspended in the air for longer. However, partially the difference can be attributed to different measurement methods and vehicles in different literature sources.

2.4. Experimental Spary Modelling

To investigate the influence of spray on vehicle visibility and safety, a reproducible spray must be simulated in a test environment. Two approaches have been identified in the literature. The first approach involves irrigating the road to mimic wet road conditions, while the second approach involves creating artificial spray directly in the air by using nozzles.

Shearman et al (1998), Borg and Vevang (2006) and Otxoterena Af Drake et al (2021) used the road-wetting approach. In particular, Otxoterena and Drake et al. (2021) used a barrier to retain water on the track and irrigated the track before each test. Other researchers used continuous track irrigation. Koppa et al. (1990) and SAE J2245 (2011) in their Recommended Practice suggest using "any system of sprinklers, irrigation pipe, or other water distribution devices that are capable of placing the water on the surface" along with a pavement slope of 1%.

Weir et al. (1978) **successfully used a perforated irrigation pipe on one side of a 1%-slope track**, as shown in Figure 10, and obtained a uniform water film with a thickness of 1.4-1.5 mm. The same approach was also employed successfully by Olson and Fry (1988). Watkins (2009) used a system of sprinklers for track wetting and reported a variation in water film thickness ranging between 1 and 3 mm. Dumas and Lemay (2004) reported that watering with sprinklers along the track did not provide a uniform and repeatable water film, whereas a 4-inch perforated pipe along the track with a 1% slope (similar to Figure 10) produced a uniform and repeatable water film.

Koppa et al. (1990) **suggest using a water film thickness of 0.5 mm** since no significant difference in generated spray was observed between depths of 0.5 mm and 1.25 mm. Similarly, Otxoterena and Drake et al. (2021) reported no substantial difference in generated spray for water depths ranging from 3 to 7 mm. SAE J2245 (2011) recommends a water film thickness between 0.5 and 1.3 mm and a water volume of up to 190 m³ per day or 190 l/min.

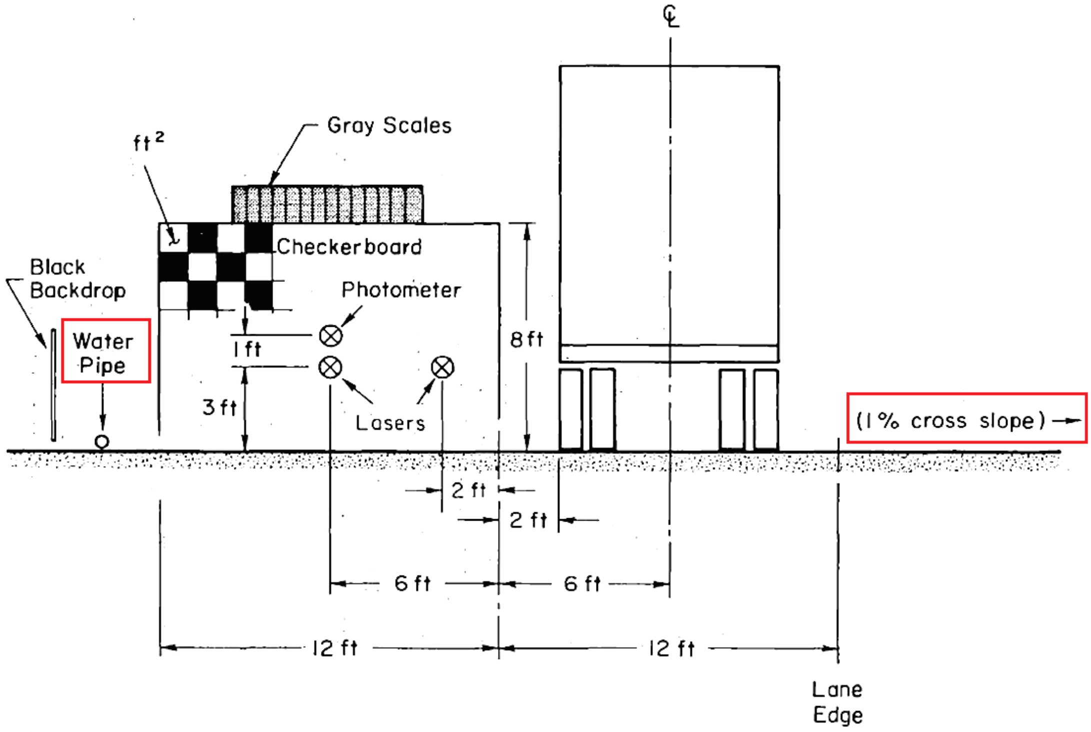

Figure 10. Test track instrumentation reproduced from Weir et al. (1978).

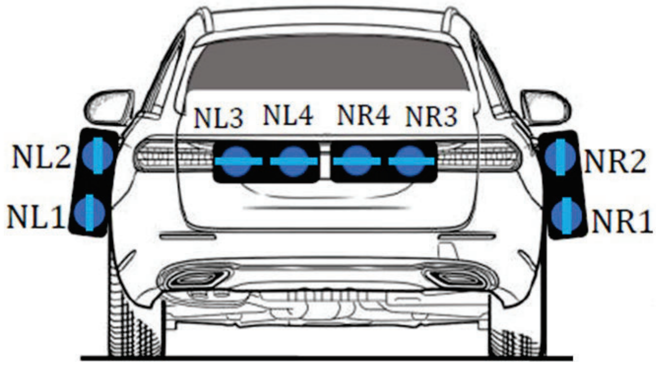

Figure 11. Car equipped with spray nozzles (labelled NL/NR 1-4) reproduced from Walz et al. (2021).

Koppa et al. (1990) recommend using a capillary gauge for water film thickness measurement. Both Koppa et al. (1990) and SAE J2245 (2011) recommend recording wind direction and speed, temperature, and humidity. Additionally, they recommend using tires with full-tread depth, inflated to the manufacturer's recommended cold inflation.

Garcia et al. (2021) used a towed water tank to release a constant water stream ahead of a tire. The tank was mounted on a truck. The authors reported that the equipment provided repeatable and reliable measurements at a vehicle speed of 25 km/h.

Gaylard and Duncan (2011) and Jilesen et al. (2013) used a wetted gravel track at Volvo's Hällered complex. Bannister (2000) used a spray grid within Volvo's wind tunnel.

Walz et al. (2021) used a spray machine mounted on a car for artificial spray generation. The car was equipped with 8 nozzles, as illustrated in Figure 11. The authors reported the successful investigation of spray effects on cameras, lidar, and radar systems.

Gaylard et al. (2017) reviewed several other studies on vehicle soiling, which could be valuable for future research, including Allan and Lilley (1983), Borg and Vevang (2006), Bouchet et al. (2004), Janson et al. (2000), Kuthada and Cyr (2006), Manser et al. (2003), Maycock (1966), Piatek and Schmitt (1998), Plocher and Browand (2014), Radovich and Plocher (2009), Spruss et al. (2010a), Spruss et al. (2010b), and Spruss et al. (2011), as well as Shearman et al. (1998).

2.5. Numerical Spray Modelling

Hagemeier et al. (2011) and Gaylard et al. (2017) provide a review and historical overview of past numerical studies on vehicle soiling. Research on rear soling and foreign soiling typically includes the numerical simulation of spray from wheels.

The work of Paschkewitz (2006) on particle dispersion in the wake of a commercial vehicle indicated that eddy-resolving flow simulations are necessary. Compared to an URANS model, using LES increased the vertical dispersion of the smallest particles by 35%. Hence, capturing the unsteady structures in the base wake is essential to obtain a realistic distribution of particles through the wake.

Kabanovs et al. (2016) and Kabanovs et al. (2017) found that neither the RANS nor URANS turbulence models, combined with a Lagrangian stochastic dispersion model, were able to provide satisfactory rear-surface deposition in the wake. This was attributed to the poor base pressure distributions predicted by these methods. Furthermore, URANS showed a much wider spreading of particles in the far wake than did RANS.

Gaylard and Duncan (2011), Jilesen et al. (2013), Gaylard et al. (2014), and Jilesen et al. (2017) all used very similar numerical approaches to simulate car soiling using LBM. Particles were released from the tire at 10-degree increments around the front or rear wheels with a mean droplet size of 0.165 mm. Gaylard and Duncan (2011) highlighted the importance of including reflections from the wheel housing in the simulation. This produced a more realistic spray with more particles being emitted from the top of the wheel, forming a large wheel spray region downstream. Additional low-velocity small particles with sizes up to 0.2 mm were released from the wheelhouse and vehicle underbody. The splashing of droplets was roughly approximated by allowing them to reflect from surfaces without breaking up. Particles with velocities near zero were considered to rest on the surface. The transient LBM results were compared with experimental soiling patterns and showed that Lagrangian particle tracking with a representation of splashing and dripping effects can produce results consistent with experimental data. Jilesen et al. (2017) used LBM-VLES simulations, releasing particles of a constant diameter of 0.165 mm from the circumference of the rear tires only, at a volumetric flow rate of 8×10^{-5} m^3/s and from a surface offset by 1 mm from the tire tread. The initial velocity of the particles was tangential to the tires, with a magnitude equal to the inlet air velocity of 30 m/s, and included a small random component of ±5m/s. The simulations utilized the Taylor analogy breakup (TAB) model, splash model, and a re-entrainment model based on a user-specified critical thickness (0.3 mm in this case).

When the film thickness reached this critical value, the excess was reintroduced into the surrounding flow as particles.

Kabanovs et al. (2019) numerically investigated wheel spray around an isolated rotating tire and a simplified SUV using IDDES with Lagrangian particle tracking. The particles were released from 26 emitter boxes around and tangential to the wheel. The authors studied various approaches for particle release, including size variations around the tire (Figure 12), dispersed size distributions, and constant sizes. They concluded that in a vehicle, droplets interact with the wheel housing, making it less critical to model the size distribution around the tire. Instead, modeling the dispersed size distribution is key. Only about 1% of spray released from the 0° to 180° region of the tire surface reached the vehicle base without interacting with the housing. Thus, modeling the tread pickup mechanism and spray generation in the wheel arch region is essential. The distribution shape agrees well with the experimental distribution of Figure 5. Note that both distributions describe the mean size of the particles.

Viner et al. (2012) (also reported in Flintsch et al. 2014) used an innovative approach for specifying boundary conditions based on physical mechanisms described by Weir et al. (1978). The simulation used RANS with discrete particle modeling (DPM). The droplets were released at various locations on the truck wheels corresponding to mechanisms such as capillary adhesion, tread pickup, bow wave, and side wave, as shown in Figure 13. Droplets were released with velocities and angles specific to each mechanism. For example, capillary adhesion droplets were released tangentially to the wheel, tread pickup droplets at an angle of 10 degrees to the ground, bow wave droplets at 35 degrees in front of the wheel, and side waves at angles along the sides of the wheel. Droplets with diameters of 0.1, 0.2, 0.5, 1, 2, and 5 mm were released at the bow wave and side wave boundaries, while droplets with diameters of 0.1, 0.2, 0.5, and 1 mm were released at the capillary adhesion and tread pickup boundaries. The study enabled visualization of the droplets' locations generated by different mechanisms, as illustrated in Figure 13.

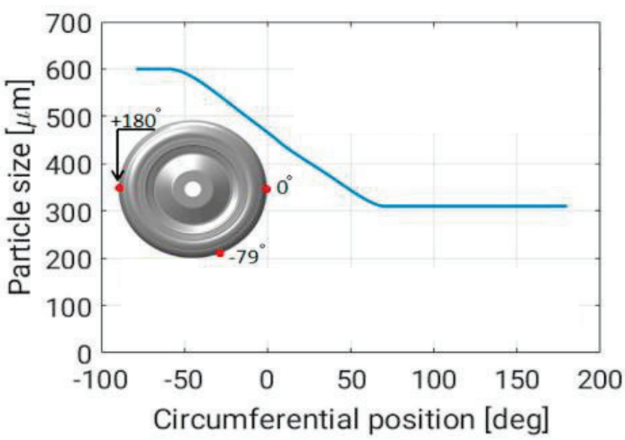

Figure 12. Particle size distribution around the wheel circumference. Reproduced from Kabanovs et al. (2019).

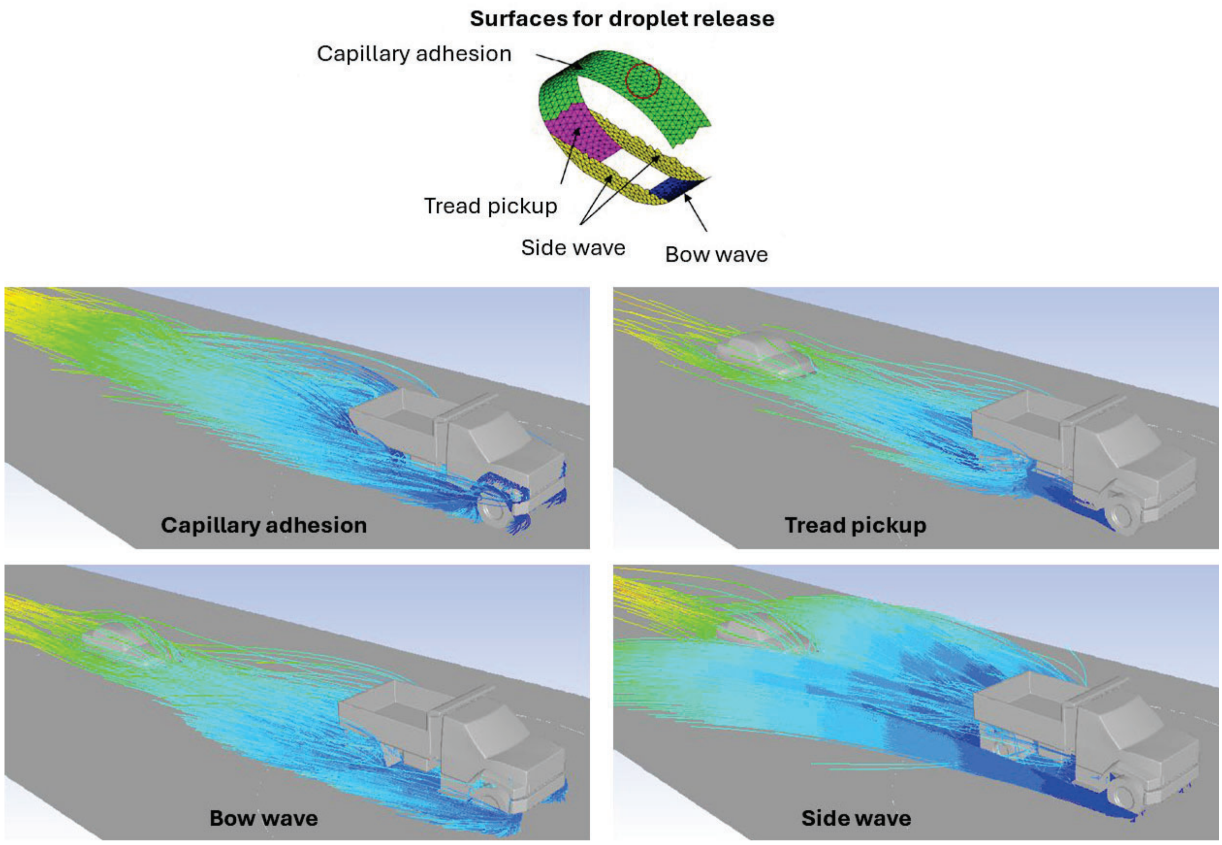

Figure 13. (Top) Surfaces for droplet release on the wheels and (bottom) particle trajectories colored by particle velocity at truck speed 48 km/h. Reproduced from Viner et al. (2012).

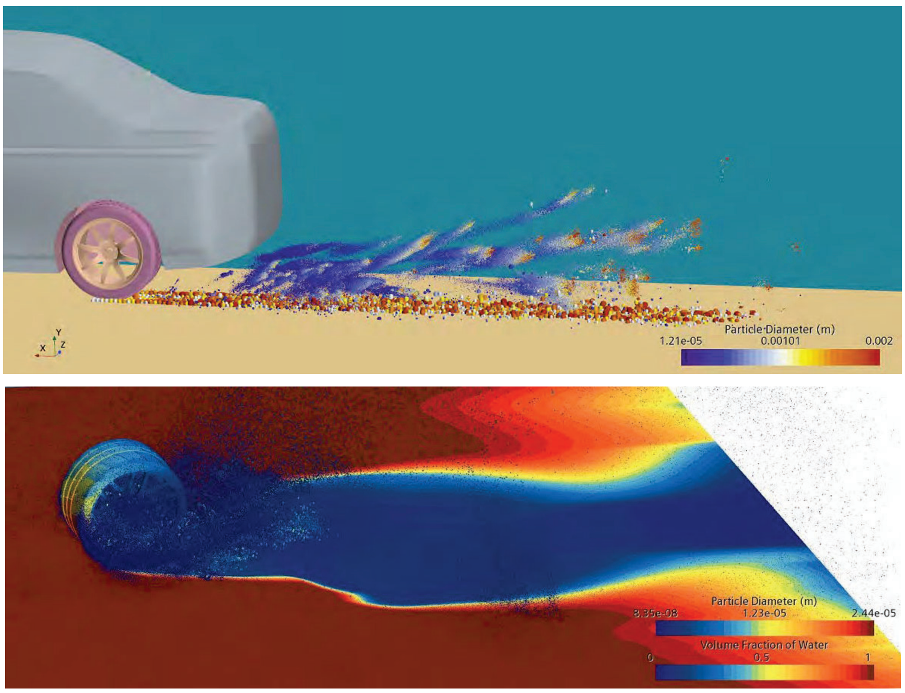

Figure 14. Chalmers' SUS calculations. Two approaches for droplet generation reproduced from Jallon (2022). (Top) Injected droplets near the ground. (Bottom) Introduced water film on the ground.

Liu et al. (2020) used a similar approach with IDDES and Lagrangian particle tracking to predict water spray deposition from the wheels of a high-speed train. Droplets with diameters of 0.2 mm were injected from the wheel tread.

Jallon (2022) presented results of spray modeling using two different approaches, as shown in Figure 14. In the first approach, Lagrangian droplets with a diameter of 2 mm were introduced 5 mm from the ground near the wheel. A model for secondary droplet breakup was used which resulted in a particle diameter change. The second approach used a 10 mm water film on the ground. The interaction between two Eulerian phases (air and water film) was modeled using the VOF-VOF phase interaction model. The interaction between air and water droplets was represented by a two-way coupling, and a stochastic secondary droplet (SSD) breakup model was used. Both methods produced promising preliminary results, though at high computational cost.

(*a*) Chalmers 200 μm

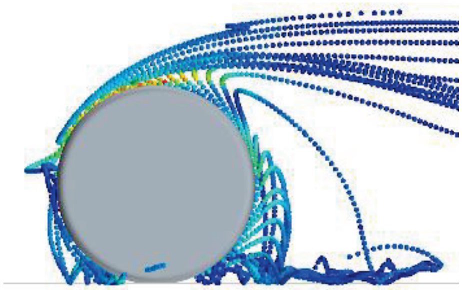

(*b*) CFD by Kabanovs etal (2019) 200 μm

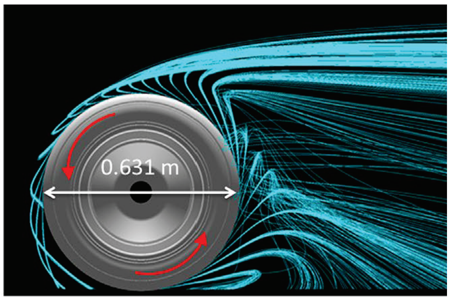

(*c*) Chalmers 500 μm

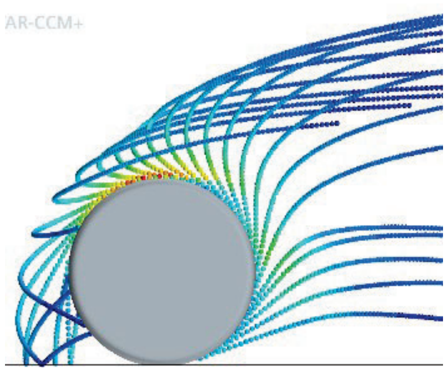

(*d*) Experiment by Kuthada & Cyr (2006)

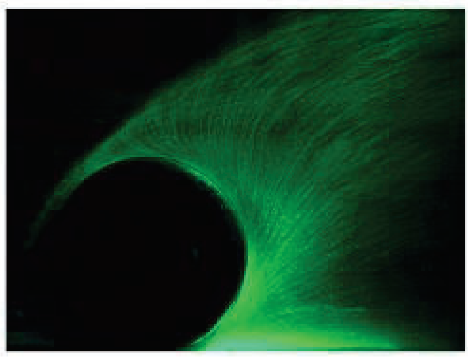

Figure 15. (a) and (c) Chalmers' SEVVOS CFD predictions of particle trajectories for: (a) 200 μm particles and (c) 500 μm particles. (b) Numerical predictions for 200 μm particles by Kabanovs et al (2019). (d) Experimental visualization by Kuthada and Cyr (2006).

Figure 15 shows numerical predictions by Chalmers for a single rotating wheel. In this case the calculations are performed for particles of single size, in one case 200 μm and in another case 500 μm. One can observe that the simulations for 200 μm particles agree very well with similar calculations of Kabanovs et al (2019). The simulations for 500 μm particles agree very well with experiments Kuthada and Cyr (2006). In experiments the particles are not of a single size but have a spatial distribution like in Fig. 5 and size distribution like in Fig. 6. The brightest particles are, however, the largest (around 500 µm) and because of this these particles are most pronounced in the experimental visualization.

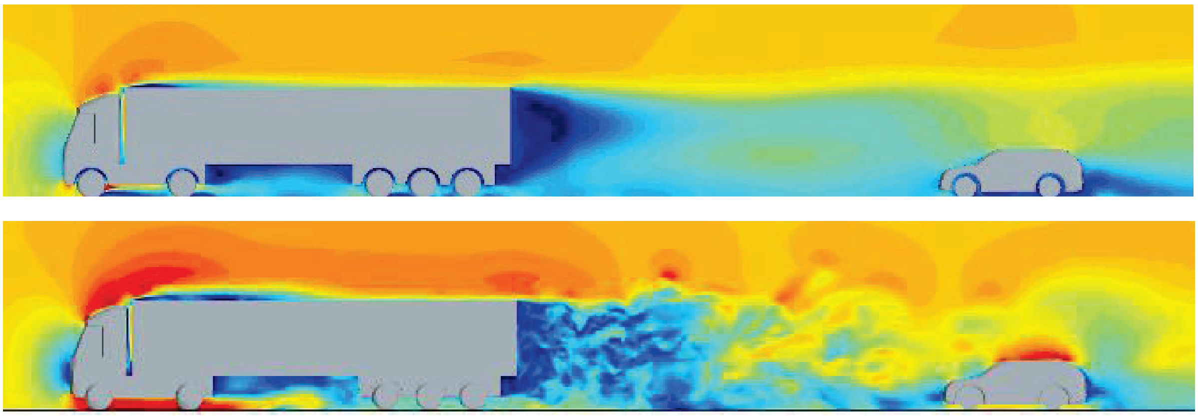

Figure 16. Chalmers' SEVVOS CFD predictions of airflow without particles. (Top) from RANS and (bottom) from DES CFD computations (color: velocity).

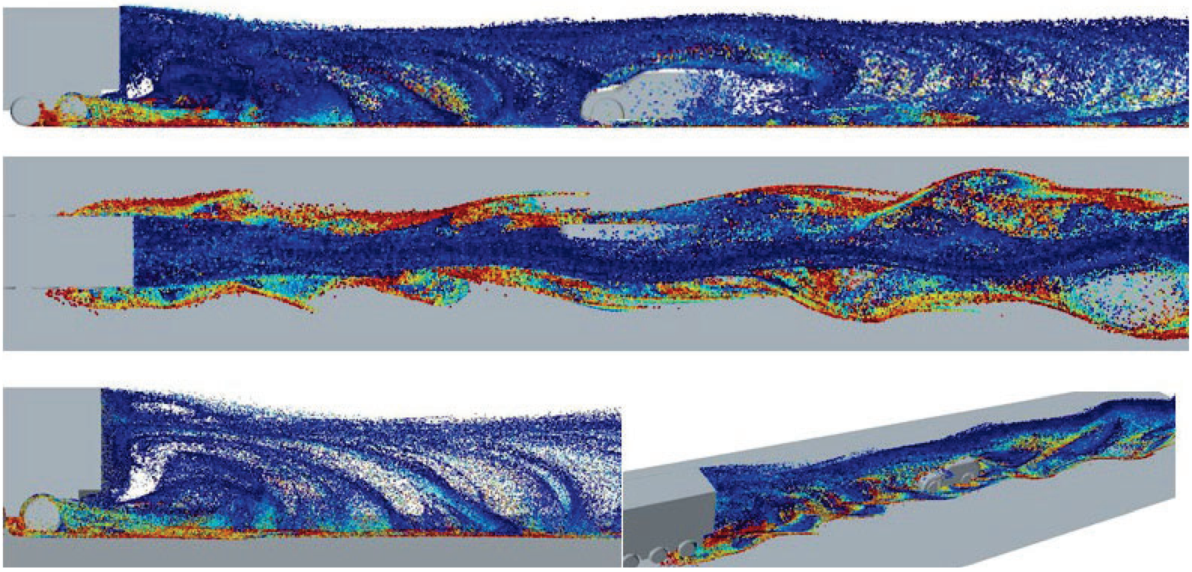

Figure 17. Chalmers' SEVVOS CFD predictions of particles behind a truck. RANS simulation with many particle sizes. Color is particle diameter.

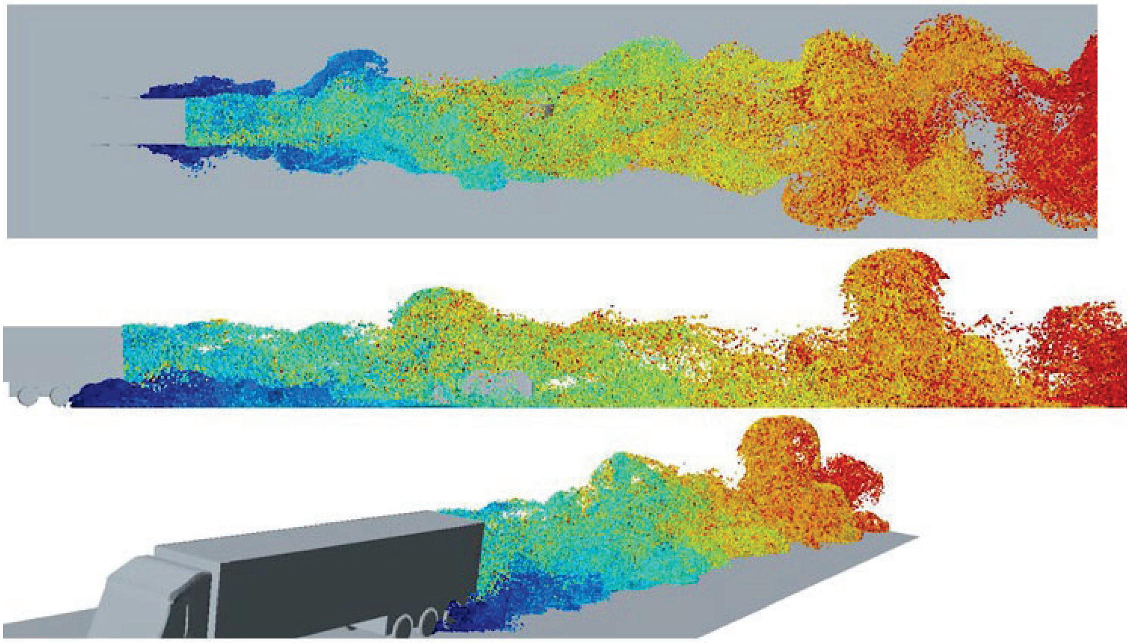

Figure 18. Chalmers' SEVVOS CFD predictions of particles behind a truck. DES simulation with many particle sizes (lognormal size distribution). Color is particle residence time.

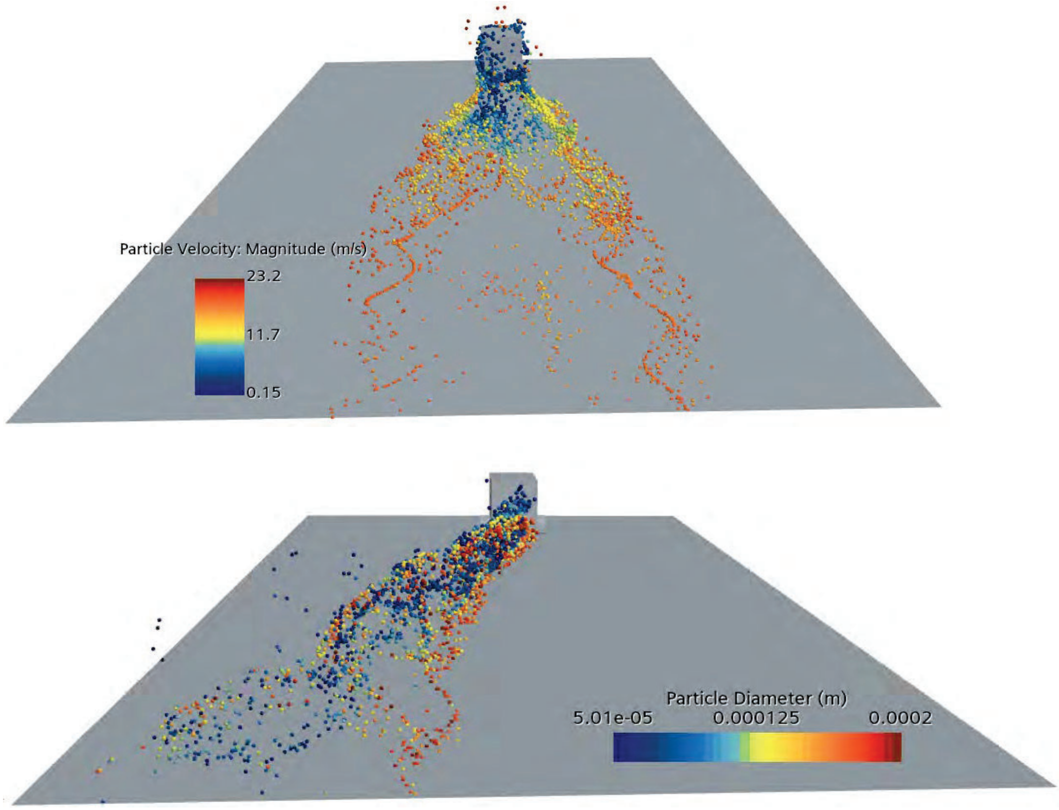

Figure 19. Chalmers' SEVVOS CFD predictions of particles behind a van with and without side wind. (Top) particle distribution without a side wind and (bottom) particle distribution with a side wind of 5 m/s.

Figure 16 shows numerical predictions by Chalmers for an airflow behind a truck and following car without particles. These simulations are performed prior injection of particles. Despite that the RANS is predicting very realistic mean flow, the unsteady flow is not captured. As our study showed, the particle injection into the RANS flow field resulted in very unrealistic particle distribution with particles concentrated near the midplane and near the ground (Figure 17). In contrast, DES simulation showed very realistic particle distribution since the particles are effectively spread out by the unsteady flow field (Figure 18).

Figure 19 shows numerical predictions by Chalmers of particles behind a van with and without side wind. The side wind is deflecting the spray particles in the wind direction. The smaller particles with longer residence time are deflected longer distance and larger particles with larger residence time are deflected shorter distance. From ballistics, see e.g. McCoy (1999), it is known that a deflection of a ballistic trajectory due to crosswind, Z is a function of the projectile's residence time in the air, t, crosswind strength, W_z, streamwise trajectory length, X, and initial streamwise velocity V_{X0} in the following way:

$$Z = W_z \left(t - \frac{X}{V_{X0}} \right)$$

Numerical studies focused on spray propagation in the far field of vehicles—relevant to visibility and safety—are very limited. Most available numerical studies of vehicle sprays focus on spray evolution near the vehicle and primarily address the problem of vehicle soiling. Chalmers' numerical simulations provide very important contribution on this subject.

2.6. Visibility Modelling

Yu and Sun (2018) used spray concentration to calculate visibility attenuation through light propagation theory. The particle concentration per m^3 was estimated from the mass flow of tread pickup and side wave sprays using theoretical models proposed by Flintsch et al. (2014) and from the Sauter mean diameter (SMD), which they assumed to be 0.5, 0.8, and 1 mm at vehicle speeds of 120, 90, and 70 km/h, respectively. The water film depth was estimated using an equation similar to Equation 1. The simulation provided changes in visibility as a function of vehicle speed and water film depth.

Wang et al. (2021) extended the approach of Yu and Sun (2018) to account for combined spray and rainfall. They found that rainfall caused an additional decrease in visibility. The simulation determined the maximum safe speed based on vehicle speed and water-film thickness.

von Bernuth et al. (2021) implemented image rendering to model primary reflections and refractions of single droplets using OpenGL. Droplets with a mean diameter of 0.2 mm were ejected from the back wheels and positioned in 3D space using simplified ballistic trajectory simulations. The simulation demonstrated the modified visibility of images due to the superimposed spray.

Ritter et al. (2022) developed an approach to generate synthetic raw sensor data for vehicle sensing systems, including cameras, lidar, and radar. Monte Carlo simulations were employed for numerical modeling of electromagnetic radiation interacting with rain, fog, and snow particles, which proved to be computationally intensive. In a second approach, a bulk light scattering model was used in conjunction with surface scattering and light sources.

Hasna et al. (2024) implemented optical simulations of rain within Ansys Speos, coupled with CFD calculations in AVL PreonLab.

Aoki et al. (2013) describe a theory for light scattering by droplets. They presented a droplet sizing method that utilizes color images of coronae observed under white-light beam illumination, also known as the corona-imaging colorimetry (CIC) method. They showed that the CIC method is technically simple while enabling accurate and instantaneous measurements of droplet sizes larger than 10 µm.

Complete optical modeling of spray based on physical principles remains computationally intensive, but simplified models such as bulk light scattering offer a promising alternative.

3. Conclusions

Water film depth can be obtained from a known rainfall intensity using an experimental pavement calibration via Equation 1. A water film depth of 0.5 mm has been successfully implemented on a test track, and a depth of 0.1 mm has been effectively utilized in a wind tunnel.

The maximum amount of splash and spray at a given water film depth can be estimated using Equation 2 based on the vehicle speed and tire width.

Generating spray through track wetting consumes approximately 10 times more water than using nozzles for spray generation. A perforated irrigation pipe provides more uniform track wetting than sprinklers.

A tire wetted with a 0.1 mm water film thickness is sufficient for spray generation via the capillary adhesion mechanism. Spray generated by tires interacts with the vehicle's underbody, wheel housings, and wheels. Spray that hits solid surfaces undergoes deposition/reflection and break-up/coalescence. Spray generated by tread pickup is thrown off close to the ground and breaks into fine spray when it strikes various vehicle parts. Both large and small droplets follow ballistic trajectories when leaving a tire; however, most large droplets quickly return to the ground, while small droplets remain suspended in the air and are carried along by airflow.

At 80 km/h, the mean droplet size measured 1 m from a vehicle is about 0.2 mm. The mean droplet size is larger near the tires (0.3 mm) and smaller further away from the vehicle (0.05–0.1 mm). Far from the vehicle, the spray droplets range in size between 0.05 and 0.5 mm in diameter.

Numerical studies focused on spray propagation in the far field of vehicles—relevant to visibility and safety—are very limited. Most available numerical studies of vehicle sprays focus on spray evolution near the vehicle and primarily address the problem of vehicle soiling.

Complete optical modeling of spray based on physical principles remains computationally intensive, but simplified models such as bulk light scattering offer a promising alternative.

Acknowledgments: Chalmers Laboratory of Fluids and Thermal Sciences. Mathis Moreau and Etienne Vimbert.

Appendix A. Mechanisms of splash and spray formation

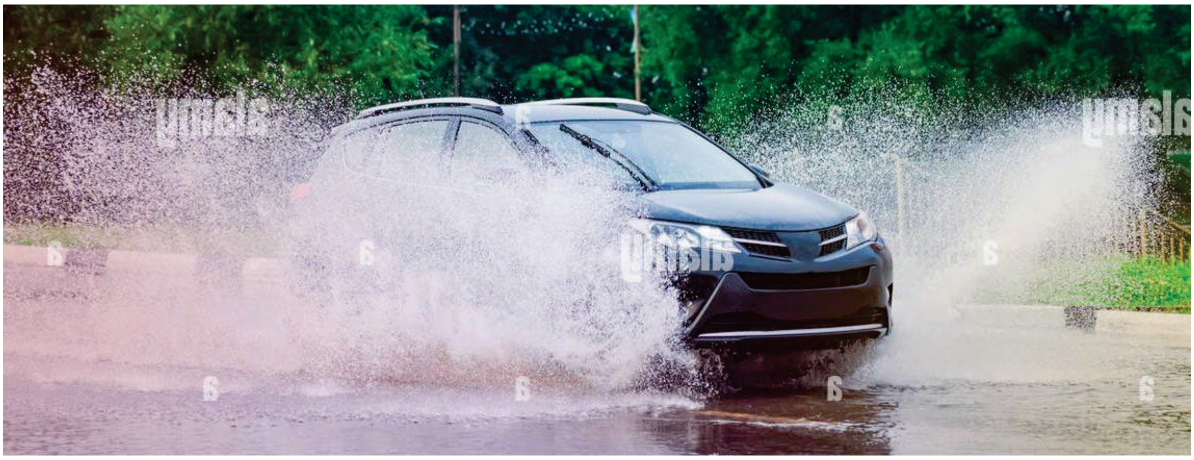

Splash with large drops at low vehicle speed and large water depth. Large side waves and bow waves are created.

Splash with large drops at 80 km/h and 3 mm water depth. Relatively large side waves are created.

Splash, spray and tread pickup on a highway. Small bow wave and side wave.

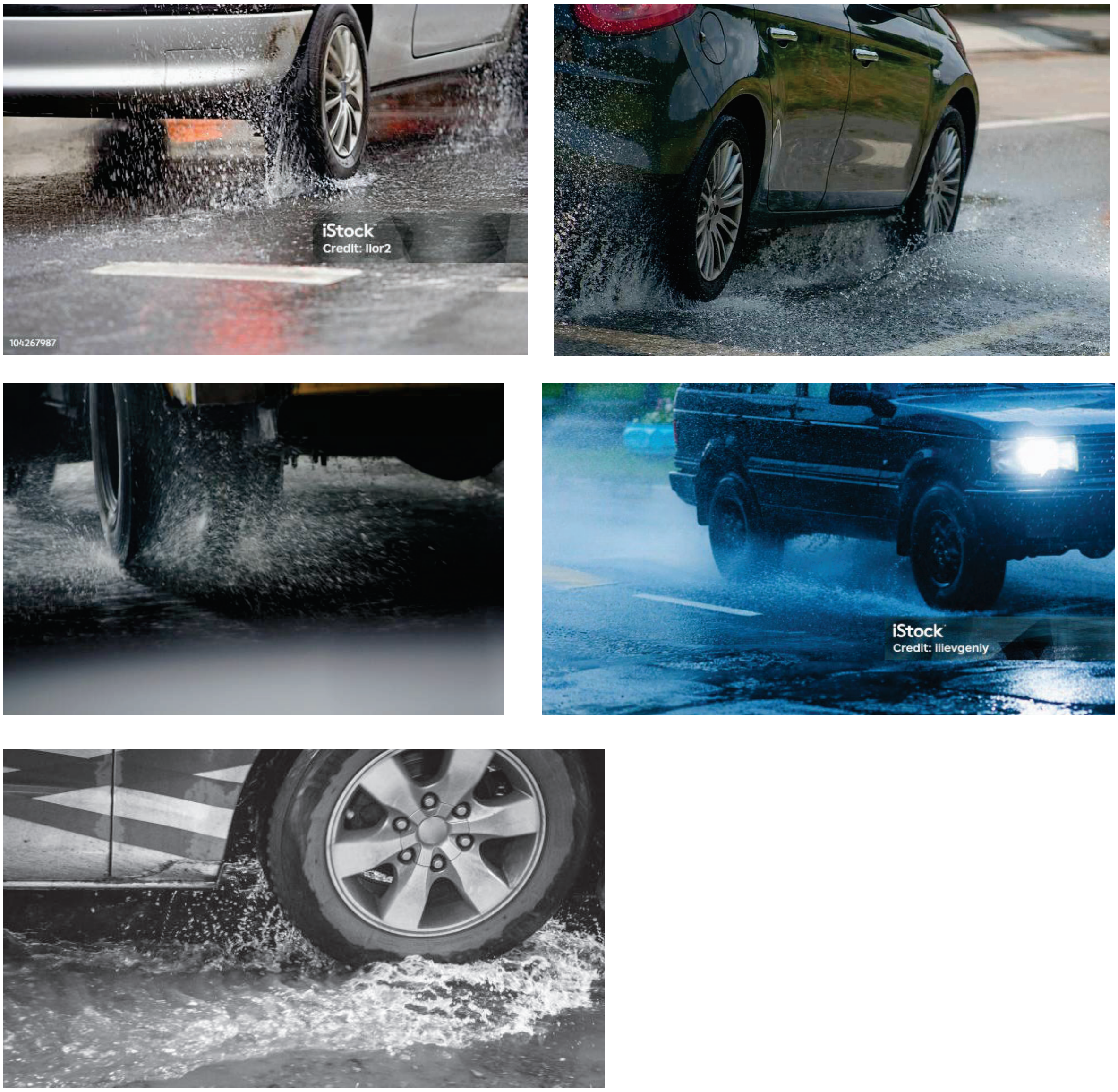

Details of tread pickup, bow wave and side wave

Appendix B. Splash and spray from trucks


iStock
Credit: adamdodd


iStock
Credit: aapsky


iStock
Credit: Yury Karamanenko


iStock
Credit: CasarsaGuru


iStock
Credit: Greenseas

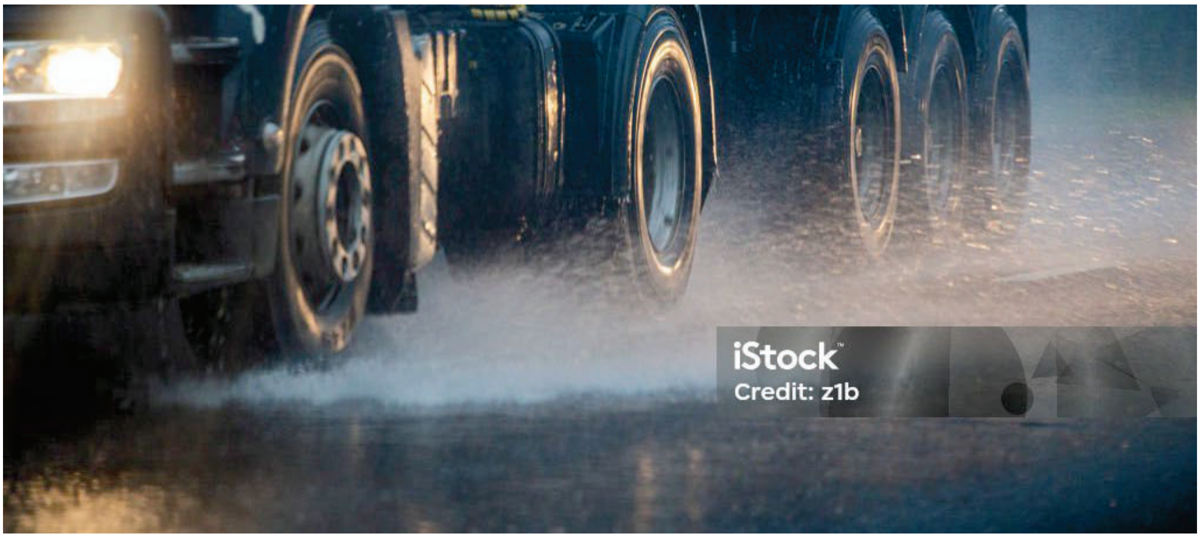
iStock
Credit: z1b


iStock
Credit: z1b


iStock
Credit: Henadzi Pechan
1352460837

References

[1] Allan J.W. and Lilley G.M. (1983) Reduction of water spray from heavy road vehicles. In: Dorgham MA and Businaro UL (eds) International conference on impact of aerodynamics on vehicle design, London, UK, 16–18 June 1982, pp. 270–307. St. Helier, Jersey: Interscience Enterprises.

[2] Anderson, D. A., Huebner, S. R., Reed, J. R., Warner, J. C., & Henry, J. J. (1998). Improved Surface Drainage of Pavements. State College, Pennsylvania: The Pennsylvania Transportation Institute.

[3] Aoki H., Moteki N., Kondo Y. (2013) Corona-Imaging Colorimetric Method for Accurate Measurement of the Size of Water Droplets in an Expansion Chamber. Aerosol Science and Technology, 47:1134–1143.

[4] Bannister M. (2000) Drag and dirt deposition mechanisms of external rear view mirrors and techniques used for optimisation. SAE paper 2000-01-0486.

[5] Best A.C. (1950) Empirical formulae for the terminal velocity of water drops falling through the atmosphere. Quarterly Journal of the Royal Meteorological Society, 76 (329), pp. 255-358.

[6] Borg A. and Vevang R. (2006) On the prediction of exterior contamination with numerical simulations (simple Lagrangian particle tracking methods with and without wall film model). In: 6th MIRA international conference on vehicle aerodynamics, pp. 380–388. Nuneaton: MIRA Ltd.

[7] Bouchet J.P., Delpech P. and Palier P. (2004) Wind tunnel simulation of road vehicle in driving rain of variable intensity. In 5th MIRA Int. Conf. on Vehicle Aerodynamics, Warwick, UK, 13–14 Oct. 2004. Nuneaton: MIRA Ltd.

[8] Clarke R.M. (1983) Heavy Truck Splash and Spray Suspension: Near- and Long-Term Solutions. SAE Paper 831178.

[9] Dumas G. and Lemay J. (2004) Splash and Spray Measurement and Control: Recent Progress in Quebec. In book: The Aerodynamics of Heavy Vehicles: Trucks, Buses, and Trains. DOI: 10.1007/978-3-540-44419-0_47.

[10] Flintsch G.W., Tang L., Katicha S., de Leon E. et al (2014) Splash and Spray Assessment Tool Development Program. Report DTFH61-08-C-00030 for the US Dept. of Transportation.

[11] Garcia, J. M. S., Garcia, M. R., & Garcia, J. A. R. (2021). Influence of Texture on Drainability, Splash and Spray in Flexible Pavements. The Baltic Journal of Road and Bridge Engineering, 16(3), 1-30. https://doi.org/10.7250/bjrbe.2021-16.530

[12] Gaylard, A. and Duncan, B. (2011) Simulation of Rear Glass and Body Side Vehicle Soiling by Road Sprays, SAE paper 2011-01-0173, https://doi.org/10.4271/2011-01-0173.

[13] Gaylard A., Pitman J., Jilesen J. et al. (2014) Insights into rear surface contamination using simulation of road spray and aerodynamics. SAE paper 2014-01-0610.

[14] Gaylard, A.P., Kirwan, K., Lockerby, D.A. (2017). Surface contamination of cars: a review. Proc. Inst. Mech. Eng. - Part D J. Automob. Eng. 231 (9), 1160–1176. https://doi.org/10.1177/0954407017695141.

[15] Gaylard A.P., Wilson A.C. and Bambrook G.S.J. (2006) A quasiunsteady description of windscreen wiper induced flow structures. In: 6th MIRA international conference on vehicle aerodynamics, Gaydon, Warwickshire, UK, 25–26 October 2006. Nuneaton: MIRA Ltd.

[16] Glantschnig W.J. and Chen S.-H. (1981) Light scattering from water droplets in the geometrical optics approximation. Applied optics, 20:14, pp 2499-2509.

[17] Hasna G., Stern D., Reitzle D., Rothmeier T. (2024) Simulation and Validation. AI-SEE project presentation.

[18] Jallon A. (2022) Eulerian-Lagrangian modeling of spray distribution behind a vehicle wheel on a wet road. Internship report for ISAE ENSMA and Chalmers.

[19] Janson J, Darrieutort L, Bannister M et al. (2000) New development and working methods used in the aerodynamic development of the new large estate. JSAE paper 20005352.

[20] Javadi, A. (2024) Flow structures on rolling wheels in various thicknesses and Reynolds numbers. Int. Comm. in Heat and Mass Transfer, Vol. 158, 107862.

[21] Jilesen J, Gaylard A, Duncan B et al. (2013) Simulation of rear and body side vehicle soiling by road sprays using transient particle tracking. SAE paper 2013-01-1256.

[22] Jilesen, J., Gaylard, A., and Escobar, J. (2017) Numerical Investigation of Features Affecting Rear and Side Body Soiling, SAE Int. J. Passeng. Cars - Mech. Syst. 10(1), doi:10.4271/2017-01-1543.

[23] Kabanovs A., Varney M., Garmory A. et al. (2016) Experimental and computational study of vehicle surface contamination on a generic bluff body. SAE paper 2016-01-1604.

[24] Kabanovs A., Garmory A., Passmore M., Gaylard A. (2017) Computational simulations of unsteady flow field and spray impingement on a simplified automotive geometry. J. of Wind Eng. & Industr. Aerodyn. 171, pp 178-195. https://doi.org/10.1016/j.jweia.2017.09.015.

[25] Kabanovs A., Garmory A., Passmore M., Gaylard A. (2019) Investigation into the dynamics of wheel spray released from a rotating tyre of a simplified vehicle model. J. of Wind Eng. & Industr. Aerodyn. 184, pp 228-246.

[26] Koppa, R.J., Pezoldt, V.J., Zimmer, R.A., Deliman, M.N., and Flowers, R. (1990) Development of a Recommended Practice for Heavy Truck Splash and Spray Evaluation. Report for Motor Vehicle Manufacturers Association of the U.S.

[27] Kuthada, T. and Cyr, S. (2006) Approaches to Vehicle Soiling. In 4th FKFS Conference on Progress in Vehicle Aerodynamics and Thermal Management: Numerical Methods. Expert–Verlag, Renningen, pp. 111–123.

[28] Liu M., Wang J., Zhu H., Krajnovic S., Zhang Y., Gao G. (2020) A numerical study on water spray from wheel of high-speed train. J. of Wind Engineering and Industrial Aerodynamics, 197. https://doi.org/10.1016/j.jweia.2019.10408.

[29] Manser M.P., Koppa R. and Mousley P. (2003) Evaluation of splash and spray suppression devices on large trucks during wet weather. Report HS-043 602, AAA Foundation for Traffic Safety, Washington, DC, USA, October 2003.

[30] Maycock G. (1966) The problem of water thrown up by vehicles on wet roads. Report 4, Road Research Laboratory, Ministry of Transport, Harmondsworth, UK.

[31] McCoy, R. (1999) Modern Exterior Ballistics: The Launch and Flight Dynamics of Symmetric Projectiles. Schiffer Publishing.

[32] Olson M.E. and Fry P.R. (1988) Highway tractor–trailer splash and spray reduction through aerodynamic design. SAE paper 881875.

[33] Otxoterena Af Drake P., Willstrand O., Andersson A., Biswanger H. (2021) Physical characteristics of splash and spray clouds produced by heavy vehicles (trucks and lorries) driven on wet asphalt. J. of Wind Engineering & Industrial Aerodynamics, 217, 104734.

[34] Parfett, A., Babinsky, H., Harvey, J.K. (2022) A study of the time-resolved structure of the vortices shed into the wake of an isolated F1 car wheel. Exp. In Fluids, 63:116. https://doi.org/10.1007/s00348-022-03458-x.

[35] Paschkewitz J.S. (2006) A comparison of dispersion calculations in bluff body wakes using LES and unsteady RANS. Report UCRL-TR-218576, Lawrence Livermore National Laboratory, Livermore, California, USA, 1 February 2006.

[36] Piatek R. and Schmitt J. (1998) Function, safety and comfort. In: Hucho W-H (ed) Aerodynamics of road vehicles: from fluid mechanics to vehicle engineering. 4th edition. Warrendale, Pennsylvania: SAE International, 1998, pp. 335–336.

[37] Pilkington, G. B. I. (1990). Splash and Spray. In W. Meyer & J. Reichert (Eds.), Surface Characteristics of Roadways (pp. 528–541). ASTM. https://doi.org/10.1520/STP23387S

[38] Plocher D.A. and Broward F.K. (2014) Comparing spray from tires rolling on a wet surface. Tire Sci Technol; 42(3): 145–165.

[39] Radovich C. and Plocher D. (2009) Experiments on spray from a rolling tire. In: Broward F, McCallen R and Ross J (eds) The aerodynamics of heavy vehicles II: trucks, buses, and trains, Lecture notes in applied and computational mechanics, Vol 41. Berlin: Springer, pp. 403–417.

[40] Resendez, Y. A., Sandberg, U., Rasmussen, R. O., & Garber, S. (2007). Characterizing the Splash and Spray Potential of Pavements. US Department of Transportation, Federal Highway Administration, 11(6).

[41] Ritter W., Bijelic M., Hasna G., Saad K., Fomin P., Prillwith G. (2022) Simulation of adverse weather as a basic requirement for the development and validation of bad weather robustness of ADS. In Proc. SIA VISION 2022.

[42] SAE J2245 (2011) Recommended Practice for Splash and Spray Evaluation SAE-J2245-201105, First issued on 1994 and stabilized in 2011, Available online: https://www.sae.org/st{and}ards/content/j2245_201105.

[43] Shearman EDR, Hoare EG and Hutton A. (1998) Trials of automotive radar and lidar performance in road spray. In: IEE colloquium on automotive radar and navigation techniques, London, UK, 9 February, pp. 10/1–10/7. London: IET.

[44] Spruss, I., Kuthada, T., Wiedemann, J., Cyr, S., Duncan, B. (2011) Spray pattern of a free rotating wheel: CFD simulation and validation. In 8th FKFS Conference on Progress in Vehicle Aerodynamics and Thermal Management. Expert–Verlag, Renningen, pp. 64–80.

[45] Spruss I., Schröck D., Kuthada T. et al. (2010) Aerodynamics as troubleshooting of wet fading. ATZ Worldwide 2010; 112(10): 22–25.

[46] Spruss I., Schröck D., Widdecke N. et al. (2010) Investigation of braking response under wet condition. In: 8th MIRA international conference on vehicle aerodynamics, Grove, Wantage, Oxfordshire, UK, 13–14 October 2010. Nuneation: MIRA Ltd.

[47] Strohbücker V., Niesner R., Schramm D., Kuthada T., Joos F. (2019) Experimental Investigation of the Droplet Field of a Rotating Vehicle Tyre. SAE Technical Paper 2019-01-5068, 2019, doi:10.4271/2019-01-5068.

[48] Viner H., Dunford A., Coyle F., Nesnas K, Hargreaves D., Parry T., Flintsch G. (2012) Development of a prediction model for splash and spray. In 7th Symposium on Pavement Surface Characteristics: SURF 2012.

[49] von Bernuth A., Volk G., Bringmann O. (2021) Augmenting Image Data Sets With Water Spray Caused by Vehicles on Wet Roads. In Proc of IEEE Intelligent Transportation Systems Conference (ITSC) 2021.

[50] Walz S., Bijelic M., Kraus F., Ritter W., Simon M., Doric I. (2021) A Benchmark for Spray from Nearby Cutting Vehicles. In Proc of 2021 IEEE Intelligent Transportation Systems Conference (ITSC), 2021.

[51] Wang S., Chen T., Yu B., Sun Y., and Qin X. (2021) Coupling impacts of spray and rainfall on road visibility and vehicle speeds: a simulation-based analysis. Can. J. Civ. Eng. 49: 1220–1230, dx.doi.org/10.1139/cjce-2021-0402.

[52] Watkins S. (2009) Spray from Commercial Vehicles: A Method of Evaluation and Results from Road Tests. In book: The Aerodynamics of Heavy Vehicles II: Trucks, Buses, and Trains. https://doi.org/10.1007/978-3-540-85070-0

[53] Weir D.H., Strange J.F., Heffley R.K. (1978) Reduction of Adverse Aerodynamic Effect of Large Trucks. U.S. Department of Transportation, Federal Highway Administration, USA, Report No. FHWA-RD-79-84, September 1978.

[54] Wäschle, A. (2007) The Influence of rotating wheels on vehicle aerodynamics—numerical and experimental investigations. SAE Technical Paper No. 2007-01-0107.

[55] Yoneda K., Suganuma N., Yanase R., Aldibaja M. (2019) Automated driving recognition technologies for adverse weather conditions. IATSS Research, 43 (4), pp. 253-262, https://doi.org/10.1016/j.iatssr.2019.11.005

[56] Yigci, I., Strohbücker, V., Kunze, M., and Schatz, M. (2024) Measurement of the Particle Distribution around the Tire of a Light Commercial Vehicle on Unpaved Roads, SAE Technical Paper 2024-01-5032, doi:10.4271/2024-01-5032.

[57] Yu B. and Sun Y. (2018) Simulation of Impact of Water-Film Spray on Visibility. J. Transp. Eng., Part B: Pavements, 144(4): 04018054.